

國立交通大學

光電工程研究所

博士論文

光固子通訊系統效能提昇之研究

Study of Performance Improvement in Soliton  
Communication System



研究生：高川原

指導教授：祁 姓 博士

溫盛發 博士

中華民國九十三年七月

光固子通訊系統效能提昇之研究

Study of Performance Improvement in Soliton  
Communication System

研究生：高川原

指導教授：祁 銓

溫盛發

Student: Chuan-Yuan Kao

Advisors: Sien Chi

Senfar Wen



博士論文

A Dissertation  
Submitted in Partial Fulfillment of the Requirements  
for the Degree of Doctor of Philosophy in  
The Institute of Electro-Optical Engineering  
College of Electrical Engineering and Computer Science  
National Chiao-Tung University  
Hsin-Chu, Taiwan, R. O. C.

中華民國九十三年七月

# 國立交通大學

## 論文口試委員會審定書

本校光電工程研究所博士班 高川原 君

所提論文 光固子通訊系統效能提昇之研究

合於博士資格標準、業經本委員會評審認可。

口試委員：

許根玉

許根玉 教授

施天從

施天從 教授

陳奇峯

陳奇峯 教授

董正成

董正成 教授

賴映杰

賴映杰 教授

指導教授：

祁 姓 溫盛發

祁 姓 教授

溫盛發 教授

所 長：

賴映杰

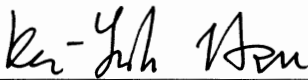
教授

中華民國 93 年 7 月 28 日

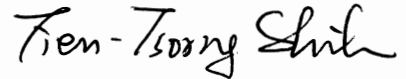
Institute of Electro-Optical Engineering  
National Chiao Tung University  
Hsinchu, Taiwan, R.O.C.

Date : July 28, 2004

We have carefully read the dissertation entitled Study of Performance Improvement in Soliton Communication System submitted by Chuan-Yuan Kao in partial fulfillment of the requirements of the degree of DOCTOR OF PHILOSOPHY and recommend its acceptance.



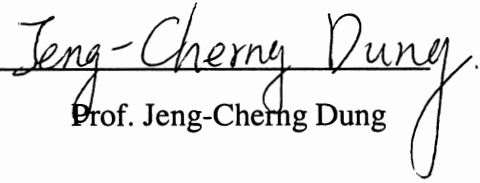
Prof. Ken-Yuh Hsu



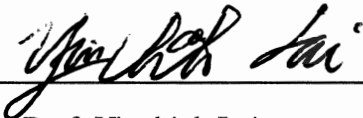
Prof. Tian-Tsorng Shi



Prof. Chi-Feng Chen

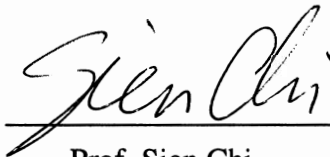


Prof. Jeng-Cherng Dung



Prof. Yinchieh Lai

Thesis Advisor :

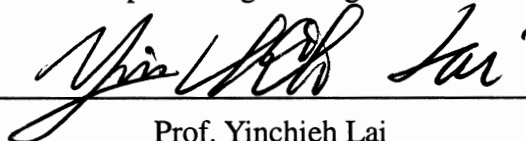


Prof. Sien Chi



Prof. Senfar Wen

Director of Institute of Electro-Optical Engineering :



Prof. Yinchieh Lai

# Study of Performance Improvement in Soliton Communication System

Author

**Chuan-Yuan Kao**

Advisors

**Sien Chi**

**Senfar Wen**

## Abstract

In this dissertation, we propose different methods to improve the performance of optical soliton communication system. First, dispersion-exponentially-decreasing fiber is used as transmission fiber between amplifier spacing. Depletion of soliton energy by the four-wave mixing between soliton and amplifier noise in the system with large amplifier spacing is studied. The improvement of the system by the use of sliding-frequency filter to reduce noise power and the depletion of soliton energy is shown. The system can further be improved by compensating for depleted soliton energy. Second, the improvements of the Q factors of 10-Gb/s soliton systems detected by adjusting detection window are studied. We have found that the optimal width of the detection window depends on the noise-induced timing jitter, noise-induced soliton energy fluctuation, amplifier noise, dispersive wave, and soliton pulsewidth. Third, the method to stabilize dispersion-managed (DM) soliton in the presence of fiber loss and optical amplifiers is presented. We optimize in-line filter bandwidth and the relating excess gain for every amplification period so that the path average pulsewidth variation is minimized and the Q factors increases. Fourth, owing to the nature of frequency chirping of a dispersion-managed (DM) soliton, one can compress its pulsewidth with a dispersion compensation fiber at

receiver so that the Q value of a DM soliton system can be improved. Numerical results show that significant improvement can be achieved with the pulse compression and proper time domain gating for filtering the radiated waves resulting from the pulse compression.



# 誌 謝

## Acknowledgement

在這不算少的日子裡，感謝祁老師與師母在課業上和生活上的教悔與關照，以及亦師亦友的溫老師在課業和生活上的提攜。若沒有他們的幫助與包容，驚頓的我將無法順利完成此論文。任何的言辭似乎都難以表達此時此刻我內心對他們的感激，惟謹以此論文獻給他們。



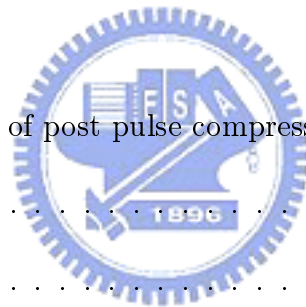
# Contents

Title Page . . . . .	i
Chinese Approval Sheet . . . . .	ii
English Approval Sheet . . . . .	iii
Chinese Abstract . . . . .	v
English Abstract . . . . .	vi
Acknowledgment . . . . .	viii
Table of Contents . . . . .	ix
List of Figures . . . . .	xi
List of Tables . . . . .	xiv
<b>1 Introduction</b>	<b>1</b>
1.1 The objective of this dissertation . . . . .	3
1.2 Numerical model . . . . .	4
<b>2 Effect of Four-Wave Mixing in Dispersion-Exponentially-Decreasing Soliton System</b>	<b>6</b>
2.1 Analysis of FWM in dispersion-exponentially-decreasing fiber . . . . .	7
2.2 Energy compensation and system performance . . . . .	10
2.3 Summary . . . . .	12
<b>3 Adjusting the Detection Window to Improve the Soliton Commu-</b>	





<b>nication System</b>	<b>19</b>
3.1 Model of system performance by using time domain gating method	20
3.2 Numerical results and discussion . . . . .	22
3.3 Summary . . . . .	25
<b>4 A Stabilization Method for Dispersion-Managed Soliton</b>	<b>32</b>
4.1 Pulse stability control by in-line filter and excess gain . . . . .	33
4.2 Numerical results . . . . .	35
4.3 Summary . . . . .	38
<b>5 Post Pulse Compression for Improving Dispersion-Managed Soli-</b>	
<b>ton Systems</b>	<b>46</b>
5.1 Theoretical model of post pulse compression . . . . .	48
5.2 Numerical results . . . . .	49
5.3 Summary . . . . .	51
<b>6 Conclusion</b>	<b>57</b>
<b>References</b>	<b>60</b>
Published Work . . . . .	66
Vita . . . . .	67



## List of Figures

2.1	Pulse shape of 10-ps soliton after propagating 10,000 km along the DEDF with $\beta_2(0) = -0.5 \text{ ps}^2/\text{km}$ is shown by solid line. The amplifier spacing is 100 km. The in-line filter of 314 GHz bandwidth is used. The pulse shape of input soliton is shown by dotted line. The pulse shape of the soliton after propagating 10,000 km without considering amplifier noise is shown by dash-dotted line. . . . .	13
2.2	Energy depletion ratio along the fiber for the case shown in Fig. 2.1. The dotted line represents the ratio of the accumulated noise energy and initial soliton energy in the absence of Kerr nonlinearity. . . .	14
2.3	Energy depletion ratio $r_d$ versus initial fiber dispersion $ \beta_2(0) $ for both 10-ps and 20-ps solitons at 10,000 km transmission distance. .	15
2.4	Allowed transmission distance versus initial fiber dispersion $ \beta_2(0) $ for (a) 10-ps and (b) 20-ps solitons. . . . .	17
2.5	soliton pulse shape for the same case as Fig. 2.1 . . . . .	18

3.1	An output pulse shape of two neighboring ONE and ZERO bits at 10,000 km for the case of soliton pulsewidth $T_s = 10$ ps. The initial pulse shape is shown by dotted line. The output pulse shapes with and without noise are shown by solid and dash-dotted lines, respectively. . . . .	26
3.2	(a) The average integrated soliton energy $\overline{E}_1$ ; (b) the standard deviation of integrated energies $\delta E_1$ , $\delta E'_1$ and $\delta E_0$ . . . . .	28
3.3	Average rms pulsewidth $T_r$ normalized by initial value $T_{ri}$ along the fiber for the case of 10-ps soliton. The cases with and without amplifier noise are shown by solid and dash lines, respectively. . . .	29
3.4	Optimal detection window $T_d$ and the corresponding Q factor for different transmission distances for the case of 10-ps soliton. . . . .	30
3.5	Q factor versus detection window $T_d$ for 10-Gbit/s bit rate and 10,000-km transmission distance. The cases of the soliton pulsewidth $T_s = 10$ ps, 15 ps, and 20 ps are shown. . . . .	31
4.1	Dispersion map. $\langle \beta_2 \rangle$ is the path average dispersion. $L_1$ and $L_2$ are the fiber length correspond to the dispersion $\beta_{21}$ and $\beta_{22}$ , respectively. The amplifier spacing is $L_a = L_1 + L_2$ . . . . .	40
4.2	The evolution of soliton energy along the transmission links, where $E_i$ represents the input initial pulse energy and represents the pulse energy at the output of every amplifier. . . . .	41
4.3	The evolutions of pulsewidth (FWHM) for the parameters in Figure 4.2. . . . .	42

4.4	The minimum path averaging pulsewidth variation $\delta$ , the filter bandwidth $B$ (normalized to 150 GHz), and the excess gain $G_e$ , along the transmission links. . . . .	43
4.5	The pulse shapes of the ideal lossless case (dashed line) and the optimized case (solid line) at 10,000km, in which the input Gaussian pulse (dotted line) is also shown for comparison. . . . .	44
4.6	The Q value of the system optimized with the above method for several dispersion maps. . . . .	45
5.1	The pulse shape and frequency chirping of a DM soliton after propagating 8,000 km . . . . .	52
5.2	The pulse shapes for the pulse before (dotted line) applying PPC and after (solid line) applying PPC. . . . .	53
5.3	The Q value and full width at half maximum (FWHM) pulsewidth versus DCF length for 8,000 km transmission distance. . . . .	54
5.4	The FWHM pulsewidth before applying PPC, and FWHM pulsewidth after applying PPC, and DCF length, as a function of transmission distance for the maximum Q value. . . . .	55
5.5	The maximum Q-value with respect to transmission distance for different schemes. Dotted line represents the DM soliton system without any optimization. Dashed line represents the case with optimal PPC. Solid line represents the case with both optimal PPC and TDG. . . . .	56

## List of Tables

4.1	The dispersion map strength correspondent to different $\beta_{11}$ and $\beta_{22}$ , $\langle\beta_2\rangle = -0.1 \text{ ps}^2/\text{km}$ , $L_1 = L_2=40 \text{ km}$ . . . . .	39
-----	---	----



# Chapter 1

## Introduction

It has been great interest in soliton optical communication systems, because they offer the highest data rate and longest transmission distance among all other communication systems [1]-[3], because soliton pulse shape is preserved owing to the balance between the nonlinear fiber effect of self-phase modulation effect and anomalous fiber dispersion during transmission [1],[4]. The soliton system is a promising backbone for modern information era. Recent experiments have demonstrated the wavelength-division-multiplexing (WDM) soliton system with 2.52 Tb/s over a distance of 320 km [5] and more than 1.0 Tb/s over a distance of 10,000 km [6] at one channel data rate of 40 Gb/s. This excellent transmission quality is due to low attenuation and distortion over a very large bandwidth in modern optical fiber waveguides. In addition, the signal can be optically amplified with either doped fiber amplifiers, such as erbium-doped fiber amplifiers (EDFAs) [3], or with Raman amplifiers [7].

The main deteriorated effects for soliton system are soliton stability problem, soliton-soliton interaction, and Gordon-Haus effect [8]. These effects limit the system performance, for examples, bit error rate (BER) and large amplifier spacing. Since the fiber loss is a strong perturbation for soliton communication system, average soliton [9]-[13] can only survive in small amplifier spacing system without pulse

distortion. Amplifier spacing is determined by soliton period which increases with fiber dispersion and decreases with the square of soliton pulsewidth. Soliton period also determines the distance for neighboring soliton collision. Gordon-Haus effect is the noise induced timing jitter which comes from the random shift of soliton carrier frequency that is due to the interaction of amplifier noise and soliton. The Gordon-Haus effect not only limits system transmission distance but also amplifier spacing because amplifier noise increases with amplifier spacing. In addition, with large amplifier spacing, the noise power introduced by the optical amplifier is significant and the signal-to-noise ratio may severely decrease. Amplifier noise can be reduced with in-line filtering [17, 20] in frequency domain and time domain. In frequency domain, conventional Fabry-Perot filter can be used. In time domain, the optical gating with sinusoidal driven electroabsorption modulator can be used. The gate function of such an optical gate can be nearly square-shaped [25]-[43].

Amplifier spacing is not only limited by amplifier noise but also the soliton stability problem. It requires that the amplifier spacing be much shorter than soliton period to maintain stable soliton transmission [14]. The amplifier spacing shorter than about 50 km is usually used in soliton system for compromising the two limitations. For the undersea optical cable system, larger amplifier spacing is desirable. We consider the soliton system with 100-km amplifier spacing, in which dispersion-exponentially-decreasing fiber (DEDFF)[15],[16] is used as the transmission medium and Fabry-Perot filter is used as the in-line filter for reducing the timing jitter [17].

## 1.1 The objective of this dissertation

The goal of this dissertation is to study the method for improving the performances of soliton optical communication systems. The performances of soliton transmission systems were evaluated by considering the noise-induced timing jitter, the fluctuation of soliton amplitude [18, 19], and the fluctuation of soliton energy. The most commonly used method of measuring the system performance in an optical transmission system is with system Q factor [21]-[23]. Q factor can be calculated by integrating signal power over a bit slot [24], which is called the integration and dump method. The integration of soliton power over a bit slot is not an optimal design because soliton energy lies within duration much smaller than a bit slot. Usually the integration time of one third bit duration is used. We found that the system Q factor can be significantly improved by optimizing the integration time [43].

It is well known that the Gordon-Haus timing jitter can be nearly eliminated in dispersion-managed(DM) long-haul soliton transmission systems [29]-[32]. There are two characteristics which limit the DM soliton system performances. First, the generation of resonant sidebands due to positive and negative dispersion links cause dispersive waves and the breathing of DM solitons [33]. If local fiber dispersion is low for increasing local soliton period, signal to noise ratio may be significantly reduced by the four wave mixing between amplifier noise and solitons. In such case, DM solitons pulse shape will be degraded seriously by noise induced dispersive waves and cause intrachannel collisions between pulses. Third-order dispersion also can enhance this effect. Second, the performances of DM



soliton systems are sensitive to the system parameters such as enhanced power, dispersion strength, dispersion map, and amplifier spacing. There are some guidelines for solving these problems [34]-[36], for example using averaging methodologies [34]-[35] to find a periodic DM soliton solution of fixed energy and fixed pulsewidth.

## 1.2 Numerical model

The governing equation for optical soliton transmission system is the modified nonlinear Schrödinger equation,

$$i\frac{\partial U}{\partial z} - \frac{1}{2}\beta_2\frac{\partial^2 U}{\partial \tau^2} - i\frac{1}{6}\beta_3\frac{\partial^3 U}{\partial \tau^3} + \gamma|U|^2U = -\frac{1}{2}i\alpha U, \quad (1.1)$$

where  $U$  is the normalized field envelope;  $\beta_2$  is the second-order dispersion;  $\beta_3$  is the third-order dispersion;  $\alpha$  is the fiber loss;  $\gamma = n_2\omega_0/cA_{\text{eff}}$ , where  $n_2$  is the Kerr coefficient,  $\omega_0$  is the carrier frequency,  $c$  is the velocity of the light in vacuum, and  $A_{\text{eff}}$  is the effective fiber cross section. In this dissertation,  $\beta_2$  is function of transmission distance  $z$  in the following chapters.

We use the split-step Fourier method to simulate the above nonlinear partial differential equations [1]. Nonlinear Schrödinger equation can be rewritten as following:

$$\frac{\partial U}{\partial z} = (\hat{D} + \hat{N})U, \quad (1.2)$$

where  $\hat{D}$  and  $\hat{N}$  stand for linear and nonlinear operators of the equation. The operators are given by

$$\hat{D} = -\frac{i}{2}\beta_2\frac{\partial^2}{\partial \tau^2} + \frac{1}{6}\beta_3\frac{\partial^3}{\partial \tau^3} - \frac{1}{2}\alpha, \quad (1.3)$$

$$\hat{N} = \gamma|U|^2, \quad (1.4)$$

for a given small distance  $h$ , the field envelope can be written as

$$U(z + h, \tau) = \exp(h\hat{D}) \exp(h\hat{N})U(z, \tau). \quad (1.5)$$

In the symmetric split-step scheme, the solution of Eq. 1.5 can be approximated by

$$U(z + h, \tau) \approx \exp\left(\frac{h}{2}\hat{D}\right) \exp\left[\int_z^{z+h} \hat{N}(z') dz'\right] \exp\left(\frac{h}{2}\hat{D}\right)U(z, \tau). \quad (1.6)$$

The solution of the exponential operator  $\exp\left(\frac{h}{2}\hat{D}\right)$  applied to the field  $U(z, \tau)$  can be calculated as

$$\exp\left(\frac{h}{2}\hat{D}\right)U(z, \tau) = \left\{ \mathcal{F}^{-1} \exp\left[\frac{h}{2}\hat{D}(i\omega)\right] \mathcal{F} \right\} U(z, \tau), \quad (1.7)$$

where  $\mathcal{F}$  denotes the Fourier transform operation. We use fast Fourier transform routine for the Fourier transform in computer code. The leading error term of split-step Fourier method is of the third order in the step size  $h$ . Therefore, the step size must be selected carefully. The optimum choice of the step size can be obtained by monitored by calculating the conserved quantities such as pulse energy, pulse width, or pulse area during transmission along the fiber.

## Chapter 2

# Effect of Four-Wave Mixing in Dispersion-Exponentially-Decreasing Soliton System

The amplifier spacing of the soliton transmission system is limited by the soliton stability and the noise induced timing jitters[8]. It requires that the amplifier spacing be much shorter than soliton period to maintain stable soliton transmission. For large amplifier spacing, the noise power introduced by the optical amplifier is significant. Therefore, the amplifier spacing shorter than about 50 km is usually used in soliton system. For the undersea optical cable system, larger amplifier spacing is desirable. In this chapter, we consider the soliton system with 100-km amplifier spacing, in which dispersion-exponentially-decreasing fiber (DEDF)[15] is used as the transmission medium and Fabry-Perot filter (FPF) is used as the in-line filter to reduce the timing jitters[17].

As fundamental soliton is maintained along DEDF, the stability condition is satisfied by using DEDF. The in-line filter stabilizes the carrier frequency of the soliton and reduces the timing jitters. It is found that there is significant four-wave mixing (FWM) between the soliton and amplifier noise in such a system because of high noise power and phase matching. The soliton-noise FWM depletes the soliton energy and the soliton broadens. The improvement of the system by the

use of sliding-frequency filter (SFF)[20] to reduce noise power and the depletion of soliton energy is considered. In addition, the system can further be improved by compensating for the depleted soliton energy.

## 2.1 Analysis of FWM in dispersion-exponentially-decreasing fiber

The pulse propagation in a DEDF can be described by the modified nonlinear Schrödinger equation

$$i\frac{\partial U}{\partial z} - \frac{1}{2}\beta_2(z)\frac{\partial^2 U}{\partial \tau^2} - i\frac{1}{6}\beta_3\frac{\partial^3 U}{\partial \tau^3} + \gamma|U|^2U = -\frac{1}{2}i\alpha U. \quad (2.1)$$

In Eq. 2.1,  $U$  is the normalized field envelope;

$$\beta_2(z) = e^{-\alpha z}\beta_2(0) \quad (2.2)$$

is the second-order dispersion, where  $\beta_2(0)$  is the initial value at every amplification stage;  $\beta_3$  is the third-order dispersion;  $\gamma = n_2\omega_0/cA_{\text{eff}}$ , where  $n_2$  is the Kerr coefficient,  $\omega_0$  is the carrier frequency,  $c$  is the velocity of the light in vacuum, and  $A_{\text{eff}}$  is the effective fiber cross section;  $\alpha$  is the fiber loss. For the numerical calculations, the carrier wavelength is taken to be  $1.55 \mu\text{m}$  and the other parameters are taken to be  $\beta_3 = 0.14 \text{ psec}^3/\text{km}$ ,  $n_2 = 3.2 \times 10^{-20} \text{ m}^2/\text{W}$ ,  $A_{\text{eff}} = 50 \mu\text{m}^2$ , and  $\alpha = 0.2 \text{ dB}/\text{km}$ . A FPF is inserted after every amplifier. We choose the bandwidth of the filter  $\Delta\nu_f = 10\Delta\nu_s$ , where  $\Delta\nu_s$  is soliton spectral width,  $\Delta\nu_s = 0.314/\tau_w$  and  $\tau_w$  is soliton pulse width (FWHM). We take  $\tau_w = 10 \text{ ps}$  and  $20 \text{ ps}$  as examples to show the results.

In Fig. 2.1 the dotted curve represents the input 10-ps soliton and the solid curve represents the pulse shape of the soliton after propagating 10,000 km along

the DEDF with  $\beta_2(0) = -0.5 \text{ ps}^2/\text{km}$ , where the gain of every amplifier is  $\exp(\alpha L_a)$  and the amplifier spacing  $L_a = 100 \text{ km}$ . The spontaneous emission factor of the amplifier  $n_{\text{sp}} = 1.2$ . The in-line filter of 314 GHz bandwidth is used. The pulse shape of the soliton after propagating 10,000 km without considering amplifier noise is shown in Fig. 2.1 by dash-dotted line for comparison. One can see that soliton energy is significantly depleted by the interaction with amplifier noise. The interaction is owing to the FWM between soliton and noise. The soliton-noise FWM is efficient because the noise power is high and the fiber dispersion is low in the considered DEDF. The asymmetric distortion of pulse shape is mainly owing to the third-order fiber dispersion and the dispersion introduced by in-line filters. To estimate the soliton energy, firstly the soliton is filtered by an ideal bandpass filter of bandwidth  $\Delta\nu_w = 4\Delta\nu_s$ . Then the soliton energy is calculated within a window of  $\Delta\tau_w = 4\Delta\tau_s$  in time domain and the calculated energy is denoted by  $E_s$ . We simulate the transmission of a single soliton 16-times to obtain the average value of the soliton energy, which is denoted as  $\bar{E}_s$ . The ratio of the energy depletion is defined as

$$r_d = 1 - \bar{E}_s/E_{s0}, \quad (2.3)$$

where  $E_{s0}$  is the initial value of soliton energy. Figure 2.2 shows the depleted energy ratio  $r_d$  along the fiber for the case shown in Fig. 2.1. The ratio  $r_n = E_n/E_{s0}$  is also shown in Fig. 2.2 by dashed line, where

$$E_n = n_{\text{sp}}(G - 1)h\nu\Delta\nu_w\Delta\tau_w z/L_a \quad (2.4)$$

is the accumulated noise energy without nonlinear mixing and  $z$  is the transmission distance. One can see that the noise energy from the optical amplifiers is

small compared with soliton energy but the depletion of soliton energy due to soliton-noise FWM is significant. From the figure,  $r_d$  almost linearly increases with distance. At the end of 10,000 km transmission,  $\bar{E}_s$  is only two thirds of  $E_{s0}$ . This manifests the pulse distortion shown in Fig. 2.1.

Figure 2.3 shows the ratio  $r_d$  with respect to  $|\beta_2(0)|$  for 10-ps and 20-ps solitons after 10,000 km transmission distance. One can see that the depletion ratio  $r_d$  can be reduced by the use of higher fiber dispersion. FWM is efficient when the soliton spectrum is near zero-dispersion frequency. The zero-dispersion frequency deviates from the carrier frequency of soliton is  $|\beta_2(z)|/\beta_3$ . Within an amplifier spacing, as  $|\beta_2(z)|$  decreases with distance, the zero-dispersion frequency moves toward the soliton frequency. Therefore soliton-noise FWM increases with distance within an amplifier spacing. The smallest fiber dispersion is  $|\beta_2(L_a)|$  at the end of every amplifier stage, and the coincident zero-dispersion frequency falls into soliton spectral width when  $|\beta_2(L_a)| = \beta_3\pi\Delta\nu_s$ . Thus the corresponding initial fiber dispersion  $|\beta_2(0)|_{\min}$  can be estimated as a lower limit

$$|\beta_2(0)|_{\min} = \left( \frac{0.314\pi\beta_3}{\tau_w} \right) e^{\alpha L_a}. \quad (2.5)$$

From the equation,  $|\beta_2(0)|_{\min} = 1.38 \text{ ps}^2/\text{km}$  and  $0.7 \text{ ps}^2/\text{km}$  for  $\tau_w = 10 \text{ ps}$  and  $20 \text{ ps}$ , respectively. Both of the depletion ratio curves in Fig. 2.3 are almost linear for  $|\beta_2(0)|$  above the lower limit values and the slopes runs up drastically for  $|\beta_2(0)|$  below them. Although larger  $|\beta_2(0)|$  leads to higher soliton power but phase matching condition is less satisfied and the efficiency of the soliton-noise FWM decreases in the case of the same pulse width. For the same  $|\beta_2(0)|$ ,  $r_d$  of 10-ps soliton is smaller than  $r_d$  of 20-ps soliton since the former has a larger

signal-to-noise ratio. If the pulse width is too short, the other effects such as third-order dispersion and self-frequency shift may deteriorate the pulse shape. From Fig. 2.3, we can see that  $r_d$  decreases as  $|\beta_2(0)|$  increases and pulse width decreases. However, in the presence of neighboring solitons and by considering noise-induced timing jitters, the system performance may not be improved as  $|\beta_2(0)|$  increases and pulse width decreases.

## 2.2 Energy compensation and system performance

To study the performance of the system, we consider the allowed transmission distance of a 10 Gb/s system for  $10^{-9}$  bit error rate (BER). 254 bits are simulated to calculate BER, where the probabilities of "ONE" and "ZERO" bits are the same. The square symbols in Figs. 2.4 (a) and (b) show the allowed transmission distances versus  $|\beta_2(0)|$  for 10-ps and 20-ps solitons, respectively. It is known that the SFF can effectively reduce noise power and timing jitters[20]. Soliton-noise FWM can also be reduced by using the SFF. The cross symbols in Figs. 2.4 (a) and (b) show the cases using the SFF, where the filter is the same as the Fabry-Perot in-line filter used above except that its central frequency is up-sliding with a rate of 3 GHz/Mm and 5 GHz/Mm in Figs. 2.4 (a) and (b), respectively. One can see that the improvement of the transmission distance ranges from 1,000 km to 2,000 km and there exists an optimum  $|\beta_2(0)|$  for the maximum transmission distance. When  $|\beta_2(0)|$  is small, soliton-noise FWM is significant. When  $|\beta_2(0)|$  is large, although the energy depletion ratio is reduced as is shown in Figs. 2.3, soliton-soliton interaction and noise-induced timing jitters are enhanced and limit

the transmission distance. By comparing Figs. 2.4 (a) and (b), for  $|\beta_2(0)| < 0.6 \text{ ps}^2/\text{km}$ , transmission distance is longer for 10-ps pulse width; for  $|\beta_2(0)| > 0.6 \text{ ps}^2/\text{km}$ , transmission distance is longer with 20-ps pulse width. Although the energy depletion ratio decreases with pulse width for the same  $|\beta_2(0)|$  as is shown in Figs. 2.3, the noise-induced timing jitter is enhanced for the soliton with shorter pulse width. The transmission distance with shorter pulse width is less than that with longer pulse width when  $|\beta_2(0)|$  is large.

To compensate for the energy depletion, we may increase amplifier gain to maintain the estimated average soliton energy  $\bar{E}_s = r_c E_{s0}$ , where  $r_c$  is the energy compensation ratio. As the energy depletion increases with distance owing to more noise power, the required amplifier gain also increases with distance. Figure 2.5 shows the pulse shape of the soliton for the same case as Figs. 2.1 except that the energy depletion is compensated and  $r_c = 1.0$ . One can see that the pulse shape is much better than that without the compensation for the energy depletion. However,  $r_c = 1.0$  may not be the optimal choice because the generated noise power through soliton-noise FWM increases with  $r_c$ . By adjusting the energy compensation ratio  $r_c$ , the maximum transmission distances for different  $|\beta_2(0)|$  by using sliding filters are shown in Figs. 2.4 by diamond symbols. For example, the optimal energy compensation ratios  $r_c$  for the case with 10-ps soliton are 0.95, 0.8, and 0.5 for  $|\beta_2(0)| = 0.2 \text{ ps}^2/\text{km}$ ,  $1.0 \text{ ps}^2/\text{km}$  and  $2.0 \text{ ps}^2/\text{km}$ , respectively. Comparing the cases without and with energy compensations shown in Figs. 2.4, we see that the transmission distance can be improved significantly when  $|\beta_2(0)|$  is not too large. When  $|\beta_2(0)|$  is large, although the soliton pulse width is maintained



better with energy compensation, the dispersive wave is larger owing to more noise power where part of the noise is converted from solitons through soliton-noise FWM. The enhancement of soliton-soliton interaction by the dispersive wave increases with  $|\beta_2(0)|$ .

### 2.3 Summary

In conclusion, we have shown the FWM between soliton and amplifier noise in the system with large amplifier spacing, where the DEDF is used as transmission fiber. When a low dispersion DEDF is used in such a system, the depletion of soliton energy due to the soliton-noise FWM is significant because of the phase matching. On the other hand, when the higher dispersion DEDF is used, the FWM is reduced, but the noise-induced timing jitter and soliton-soliton interaction increase. Therefore, there exists an optimum fiber dispersion for the maximum transmission distance. The improvement of the soliton system by using the SFF and by compensating for depleted soliton energy are also shown.

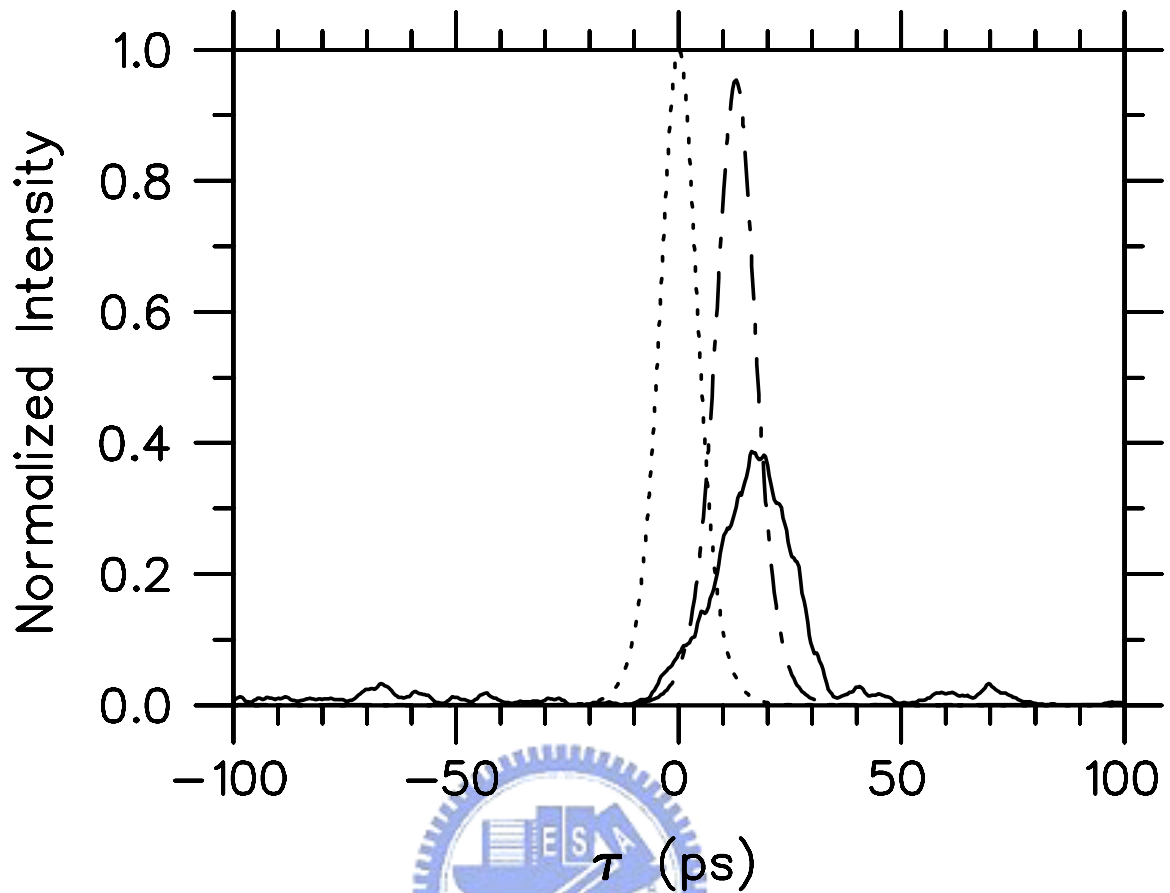


**Figure 2.1**

Pulse shape of 10-ps soliton after propagating 10,000 km along the DEDF with  $\beta_2(0) = -0.5 \text{ ps}^2/\text{km}$  is shown by solid line. The amplifier spacing is 100 km. The in-line filter of 314 GHz bandwidth is used. The pulse shape of input soliton is shown by dotted line. The pulse shape of the soliton after propagating 10,000 km without considering amplifier noise is shown by dash-dotted line.

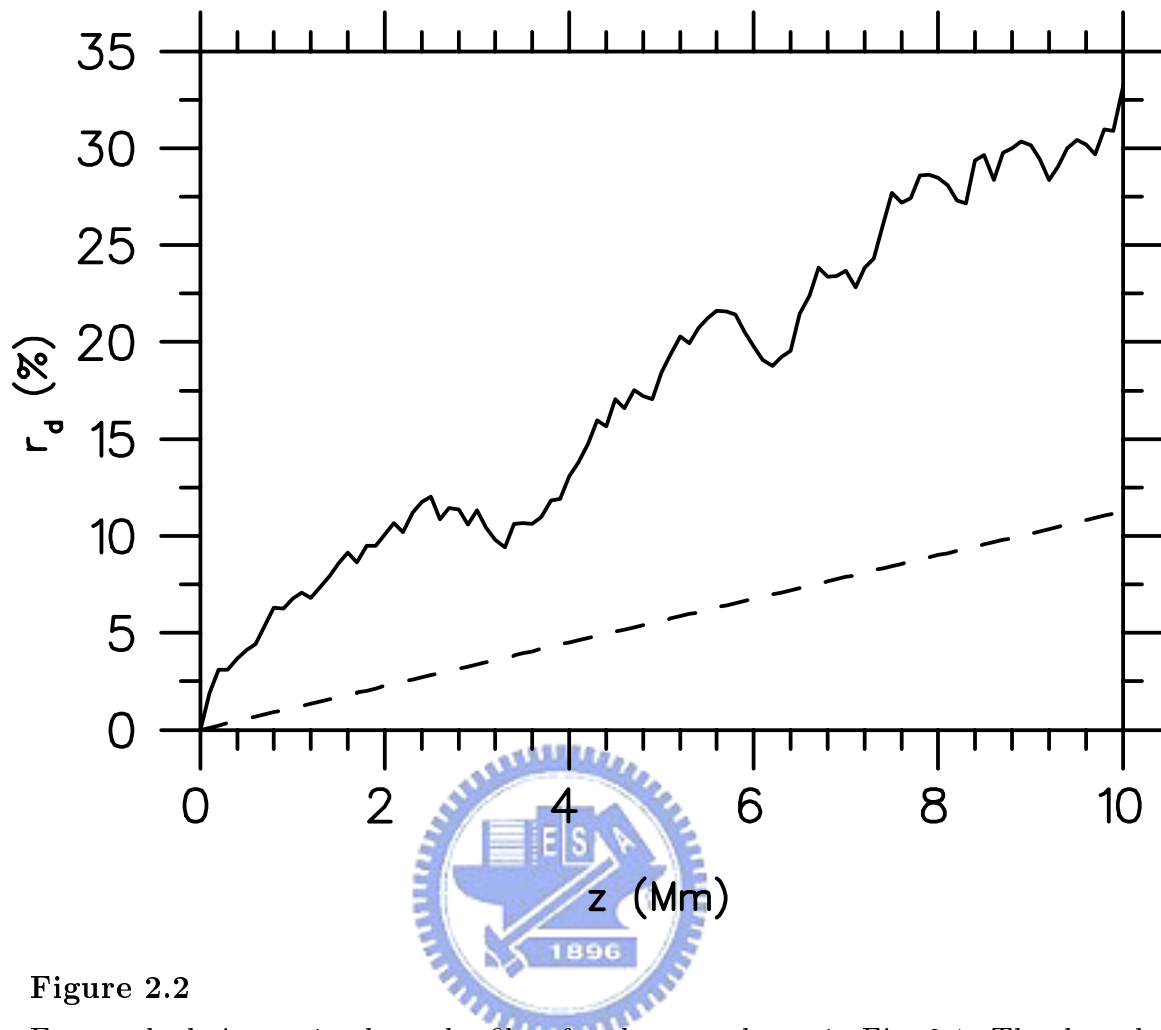


**Figure 2.2**

Energy depletion ratio along the fiber for the case shown in Fig. 2.1. The dotted line represents the ratio of the accumulated noise energy and initial soliton energy in the absence of Kerr nonlinearity.

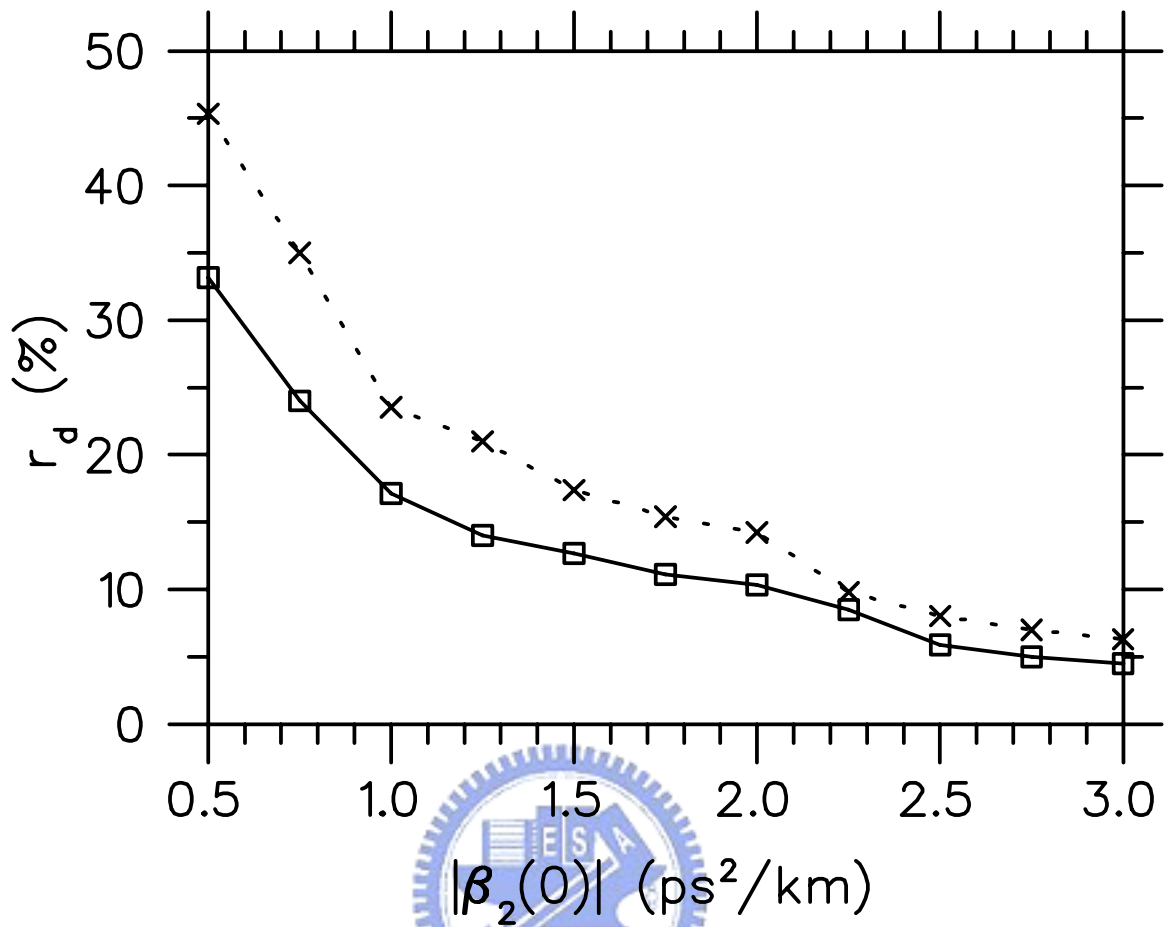


**Figure 2.3**

Energy depletion ratio  $r_d$  versus initial fiber dispersion  $|\beta_2(0)|$  for both 10-ps and 20-ps solitons at 10,000 km transmission distance.

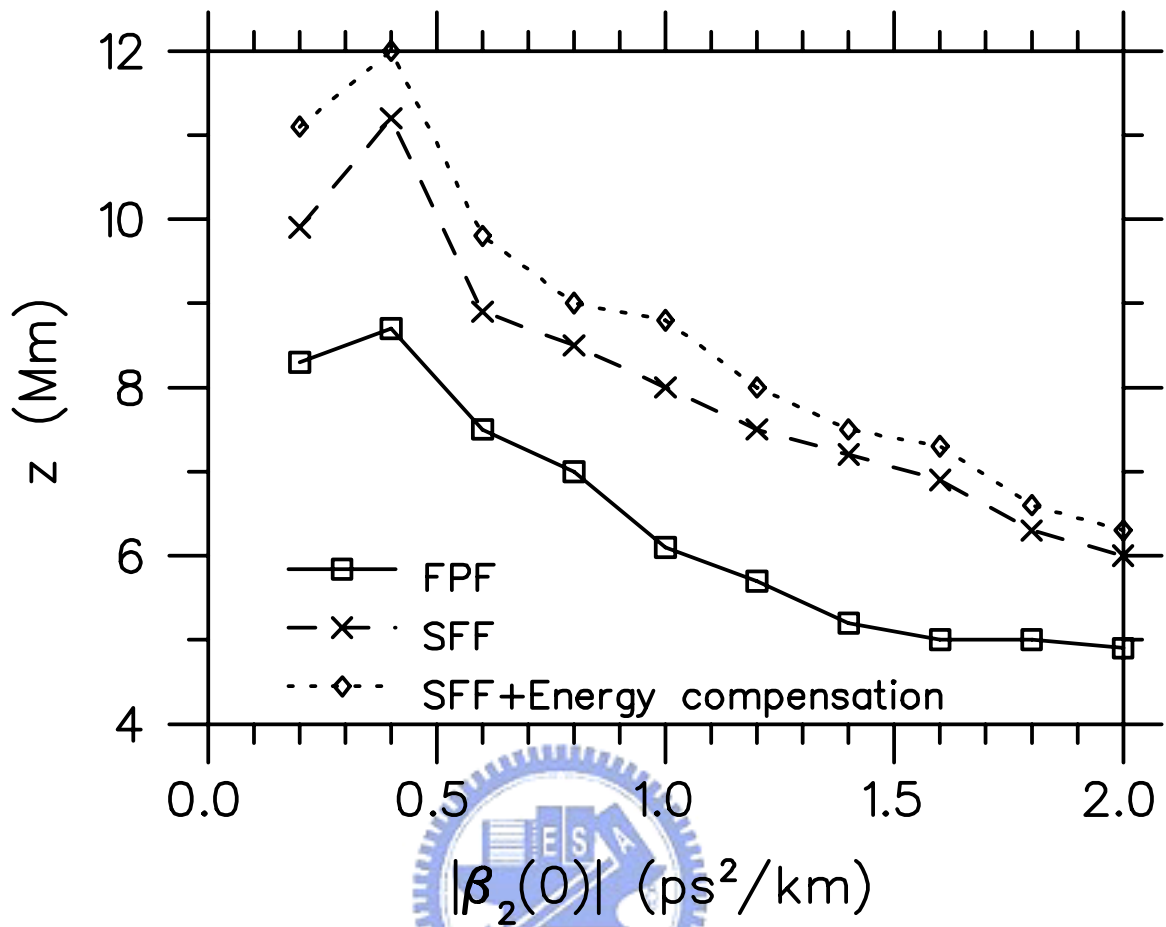
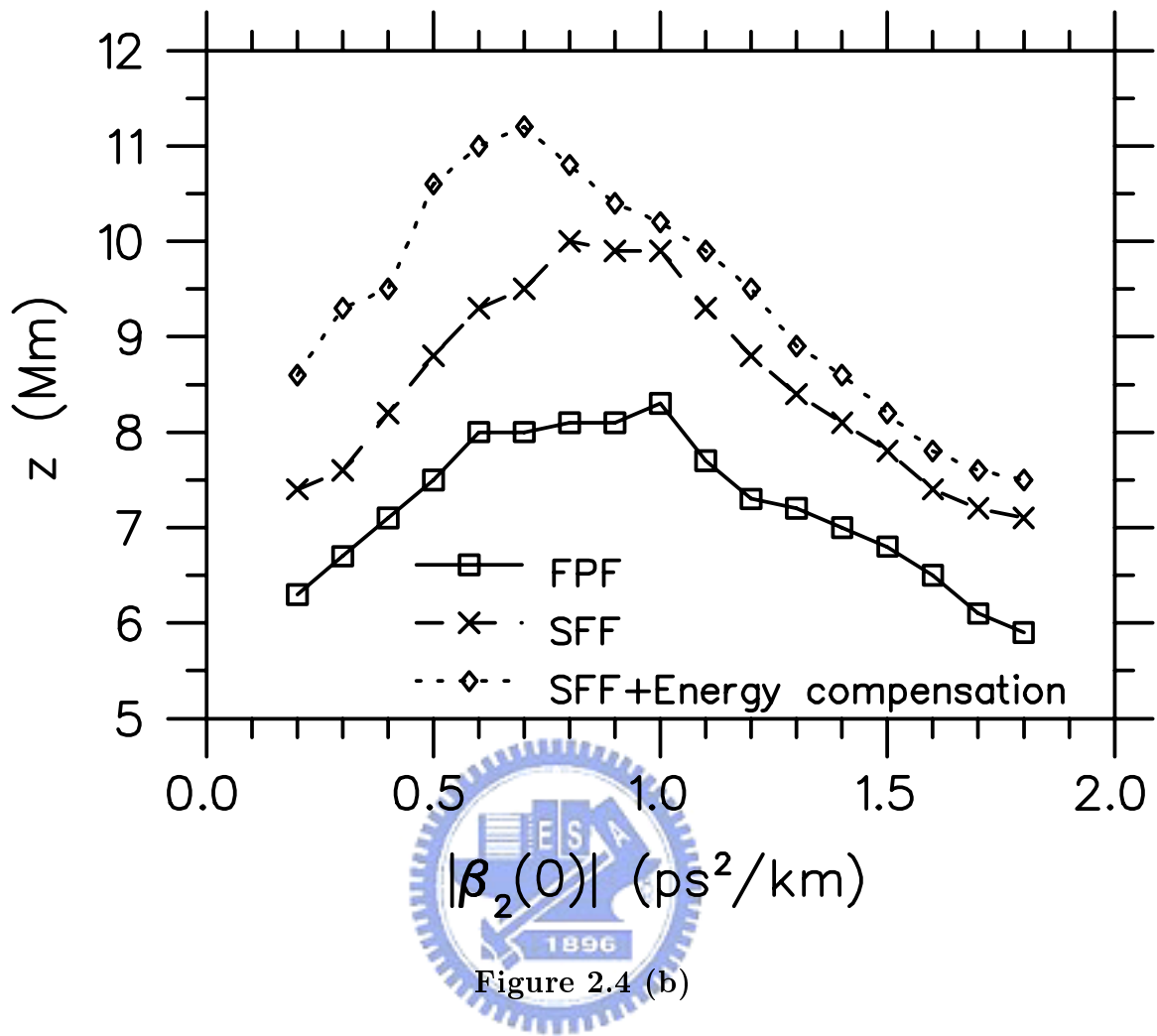
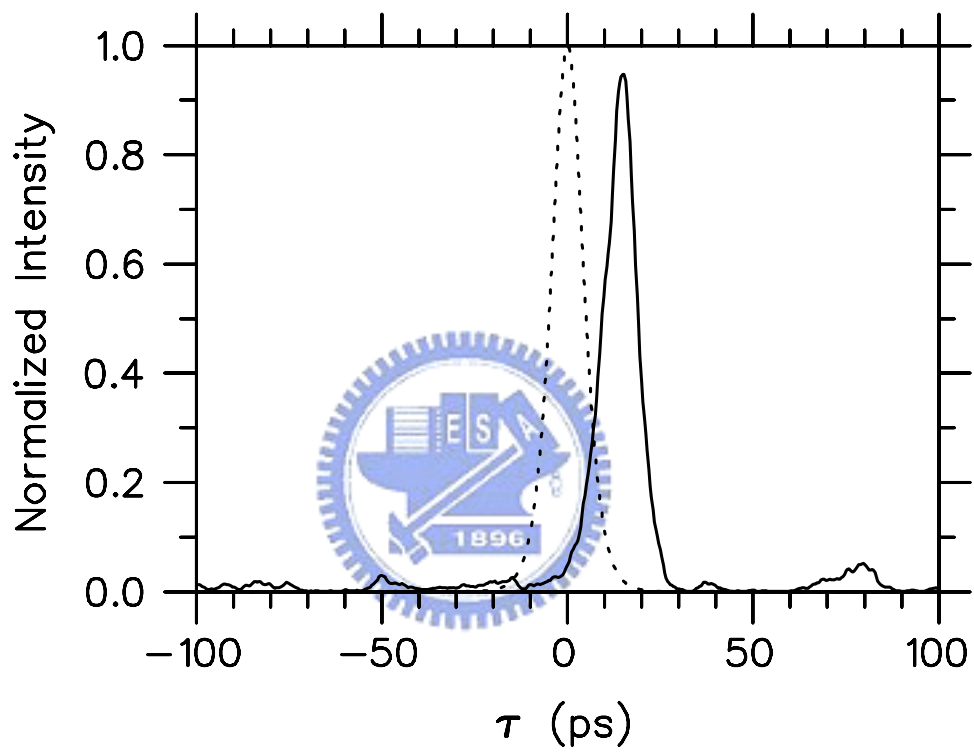


Figure 2.4 (a)



**Figure 2.4**

Allowed transmission distance versus initial fiber dispersion  $|\beta_2(0)|$  for (a) 10-ps and (b) 20-ps solitons.



**Figure 2.5**

Soliton pulse shape for the same case as Fig. 2.1 except that the energy depletion is completely compensated

## Chapter 3

# Adjusting the Detection Window to Improve the Soliton Communication System

The performances of soliton transmission systems were evaluated by considering the noise-induced timing jitter [8], the fluctuation of soliton amplitude [18],[19], and the fluctuation of soliton energy. The most commonly used method of measuring the system performance in an optical transmission system is the decision circuit method of measuring Q factor [21],[22]. The Q factor can be calculated by integrating its power over a bit slot [24], which is called the integration and dump method. The integration of soliton power over a bit slot is not an optimal design because soliton energy lies within a duration much smaller than a bit slot. It has been reported that the in-line optical gate in time domain could reduce ASE noise [25]. The optical gate can be realized by a sinusoidal driven electroabsorption modulator and the gate function is nearly square-shaped [26],[27],[28].

Considering such an optical gate is placed before the photodiode of the receiver, only the soliton power within the gate time is able to arrive at the photodiode. Then the received signal is integrated over a bit duration in the receiver. Therefore, the optical gate together with the receiver circuit function as an integrator which integrates the soliton power over a duration of the gate time. We call the gate time as detection window. When the detection window is less than a bit slot, a fraction



of noise energy can be excluded without the expense of signal energy. On the other hand, with too small an detection window like sampling the signal's amplitude at bit centrum, the system performance may suffer from the noise-induced timing jitter. The dependence of the system performance on detection window has not been considered in literatures. In this chapter we will study the improvements of the Q factors of a soliton systems by adjusting the detection window, called time domain gating (TDG) method,

### 3.1 Model of system performance by using time domain gating method

The modified nonlinear Schrödinger equation, as in Eq. 2.1, describing the soliton propagation in a fiber is numerically solved. We take the carrier wavelength  $\lambda = 1.55 \mu\text{m}$ , the second-order fiber dispersion  $\beta_2 = -0.25 \text{ ps}^2/\text{km}$ , the third-order fiber dispersion  $\beta_3 = 0.14 \text{ ps}^3/\text{km}$ , the Kerr coefficient  $n_2 = 2.7 \times 10^{-20} \text{ m}^2/\text{W}$ , the effective fiber area  $A_{\text{eff}} = 50 \mu\text{m}^2$ , and the fiber loss  $\alpha = 0.2 \text{ dB}/\text{km}$ . The soliton system of 10-Gb/s bit rate is considered and its bit slot  $T_b = 100 \text{ ps}$ . The soliton pulsewidth  $T_s$ (FWHM) and the transmission distance  $L_t$  are varied. The soliton is amplified every 50 km and the spontaneous emission factor  $n_{\text{sp}}$  of an optical amplifier is assumed to be 1.2. An in-line Fabry-Perot filter is inserted after every amplifier to reduce the amplified spontaneous emission (ASE) noise and noise-induced timing jitter, where the filter bandwidth is optimized. A second-order Butterworth electric filter with a narrower bandwidth  $\Delta\nu_f$  in the receiver is used to further reduce noise [9,10]. The accumulated ASE noise is detrimental

for optical amplified long links [18], and the shot noise and thermal noise in the receiver are negligible. For the cases shown in this paper,  $\Delta\nu_f$  is also optimized. The bit energy is obtained by integrating the amplitude of the filtered signal over a bit slot in which its centrum coincides the bit centrum. The gate function of the detection window is modeled by a fifth-order super-Gaussian function

$$G(T) = \exp \left[ -\frac{1}{2} \left( \frac{T}{T_d} \right)^{2m} \right], \quad (3.1)$$

where  $T_d$  is the detection window and  $m = 5$ . The system performance can be evaluated by bit error rate (BER) which is given by [28]

$$\text{BER} = \frac{1}{4} \left[ \text{erfc} \left( \frac{\bar{E}_1 - E_D}{\delta E_1 \sqrt{2}} \right) + \text{erfc} \left( \frac{E_D - \bar{E}_0}{\delta E_0 \sqrt{2}} \right) \right], \quad (3.2)$$

where

$$\text{erfc}(x) = \frac{2}{\sqrt{\pi}} \int_x^{\infty} e^{-y^2} dy \quad (3.3)$$

is the complementary error function. In Eq. 3.2,  $E_D$  is the decision threshold;  $\bar{E}_1$  and  $\bar{E}_0$  are the average integrated energies of ONE and ZERO bits, respectively;  $\delta E_1$  and  $\delta E_0$  are the standard deviations of energies of ONE and ZERO bits, respectively. The Q factor of the soliton system can be evaluated by BER, which is

$$Q = \sqrt{2} \text{erfc}^{-1}(2 \cdot \text{BER}). \quad (3.4)$$

For  $\text{BER} = 10^{-9}$ ,  $Q = 6$ . For a given detection window  $T_d$ , the decision threshold  $E_D$  is optimized for the minimum BER or the maximum Q. We use 1024 sample bits of equal probable ONE and ZERO bits to calculate the Q factor.

## 3.2 Numerical results and discussion

Figure 3.1 shows an output of two neighboring ONE and ZERO bits for the case of transmission distance  $L_t = 10,000$  km and soliton pulsewidth  $T_s = 10$  ps. In Figure 3.1, the initial pulse shape and the output pulse shape without ASE noise are shown for comparison. One can see that, in the absence of ASE noise, soliton broadens and the displacement of the soliton is due to the third-order fiber dispersion and filters. In the presence of ASE noise, soliton further broadens and the displacement of the soliton is due to noise-induced timing jitter in addition to the third-order fiber dispersion and filters. In the presence of ASE noise, the beating and the nonlinear interaction between ASE noise and soliton lead to the distortion of output pulse shape, especially on the pedestal of the soliton, and the fluctuation of integrated energy. There is significant dispersive wave radiated from the soliton owing to the nonlinear interaction. One can see that the output soliton energy with ASE noise is less than that without ASE noise. The noise-induced soliton energy fluctuation and timing jitter are the main origins of the BER of ONE bits. Because the power of dispersive wave is low and the nonlinear interaction between ASE noise and dispersive wave is weak, the beating between ASE noise and dispersive wave is the main origin of the BER of ZERO bits and is also an origin of the BER of ONE bits when detection window  $T_d$  is large.

Figure 3.2 (a) shows the average integrated soliton energy  $\overline{E}_1$  versus detection window  $T_d$  at 10,000 km for the case of  $T_s = 10$  ps. The data shown in the figure is normalized by the average energy within a bit slot  $\overline{E}_{1U}$ , *i.e.*,  $\overline{E}_{1U} = \overline{E}_1(T_d = T_b)$ . The dash line represents the case that the center of the detection window is at the

soliton peak in order to exclude the effect of timing jitter. Solid line represents the case that the center of the detection window is at bit centrum and the effect of timing jitter is included. We can see that, when  $T_d$  is small, the average integrated soliton energy  $\overline{E}_1$  including the timing jitter is less than that without the timing jitter. When  $T_d$  is larger than about 25 ps, the effect of timing jitter on the average soliton energy can almost be neglected. Figure 3.2 (b) shows  $\delta E_1$  and  $\delta E_0$  versus  $T_d$  for the same case shown in figure 3.2 (a). One can see that  $\delta E_0$  slowly increases with  $T_d$ .  $\delta E_1$  rapidly decreases as  $T_d$  increases when  $T_d$  is less than about 20 ps mainly because of noise-induced timing jitter. This shows that the effect of timing jitter is more tolerable with larger detection window. The noise-induced soliton energy fluctuation also contributes to  $\delta E_1$ , which can be observed by comparing  $\delta E_1$  to  $\delta E'_1$  shown in the figure by dash-dot line.  $\delta E'_1$  is the standard deviation of integrated energies of ONE bits calculated by taking the center of the detection window at the soliton peak in order to exclude the effect of timing jitter. When  $T_d$  is larger than 25 ps,  $\delta E_1$  increases with  $T_d$  that is due to the ASE noise and dispersive wave.

For the integration and dump method, the optimal  $T_d$  relates to soliton pulsewidth. Figure 3.3 shows the increase of average root-mean-square (rms) pulsewidth  $T_r$  normalized by initial rms pulsewidth  $T_{r,i}$  along the fiber for the case of 10-ps soliton. In figure 3.3 both cases with and without amplifier noise are shown. As is explained previously, ASE noise enhances soliton broadening. We optimize  $T_d$  along the transmission distances and the results are shown in figure 3.4, where the corresponding Q are also shown. One can see that the optimal  $T_d$  increases with

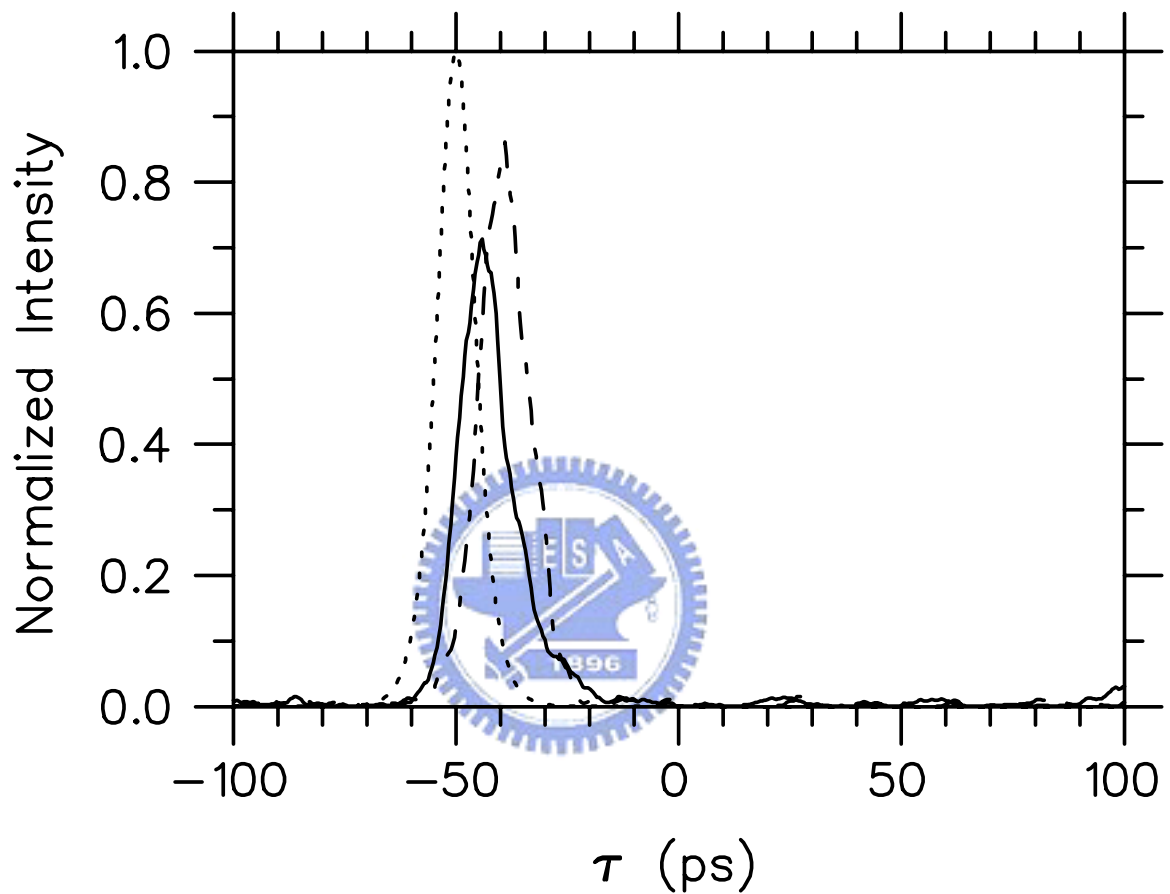
pulsewidth. A larger pulsewidth requires a wider detection window in order to reduce the degradation of Q that is due to noise-induced timing jitter and soliton energy fluctuation.

Figure 3.5 shows Q versus  $T_d$  for  $L_t = 10,000$  km and  $T_s = 10$  ps, 15 ps, and 20 ps. The optimal  $T_d = 35$  ps, 47 ps, and 55 ps for  $T_s = 10$  ps, 15 ps, and 20 ps, respectively. For the considered cases, the optimal  $T_d$ 's are about three times of the initial pulsewidth. One can see that the optimal  $T_f$  for the maximum Q factor increases with initial soliton pulsewidth. For a small detection window, Q factor is mainly deteriorated by ONE bits that is due to noise-induced timing jitter and soliton energy fluctuation. When  $T_d$  is much less than the pulsewidth, the detection method in fact becomes the sampling method in which the Q factor is calculated by sampling the signal's amplitude at bit centum. The result shows that the sampling method is not the best detection method to obtain the maximum Q factor. For a larger detection window ( $T_d > 22$  ps in the case of  $T_s = 10$  ps), Q is mainly degraded by ZERO bits because ZERO bits contain significant dispersive waves which can be clearly observed in figure 3.1. Again, from the results shown in figure 3.5, the Q measured by sampling method are smaller than the maximum Q measured by the integration and dump method. With the integration and dump method, the maximum Q is higher for shorter initial pulsewidth because the signal-to-noise ratio is higher for the soliton of shorter pulsewidth.

### 3.3 Summary

In conclusion, the improvements of the Q factors of 10-Gb/s soliton systems detected by TDG method are studied. The optimal detection window depends on the noise-induced timing jitter, noise-induced soliton energy fluctuation, ASE noise, dispersive wave, and soliton pulsewidth. The contribution of BER from ONE bits is slightly larger than ZERO bits with the optimal detection window. It is found that the optimal detection window by the integration and dump method is about three times of the initial soliton pulsewidth for the considered cases.





**Figure 3.1**

An output pulse shape of two neighboring ONE and ZERO bits at 10,000 km for the case of soliton pulsewidth  $T_s = 10$  ps. The initial pulse shape is shown by dotted line. The output pulse shapes with and without noise are shown by solid and dash-dotted lines, respectively.

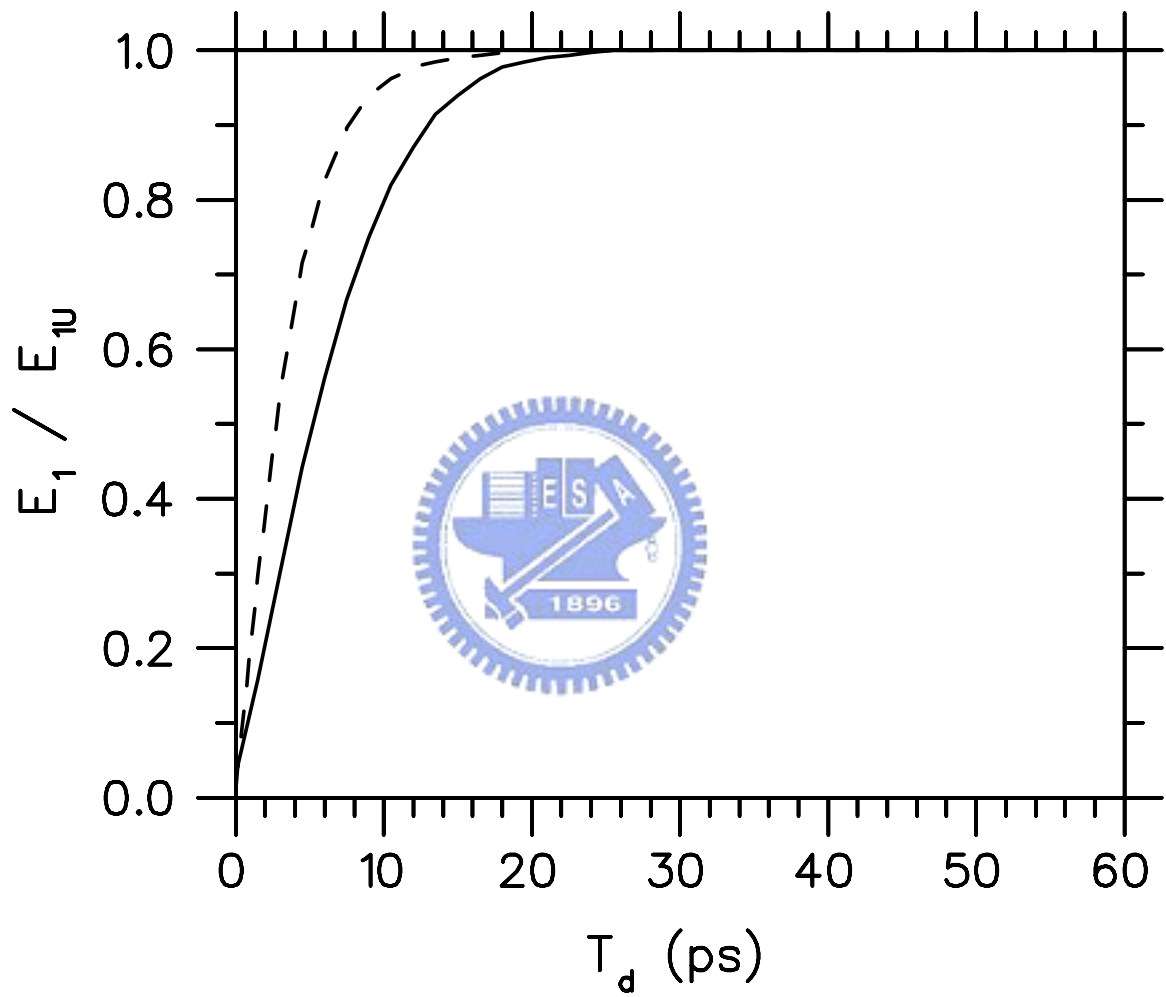


Figure 3.2 (a)



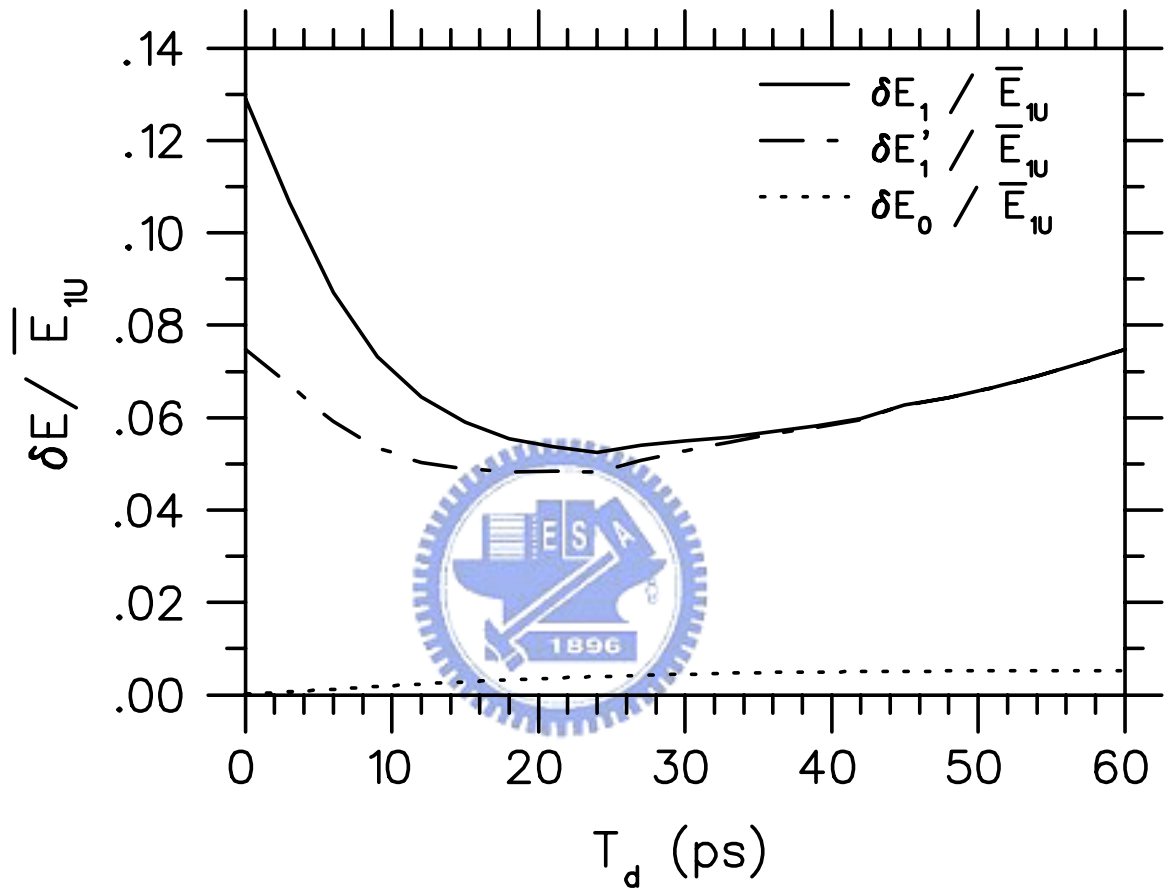
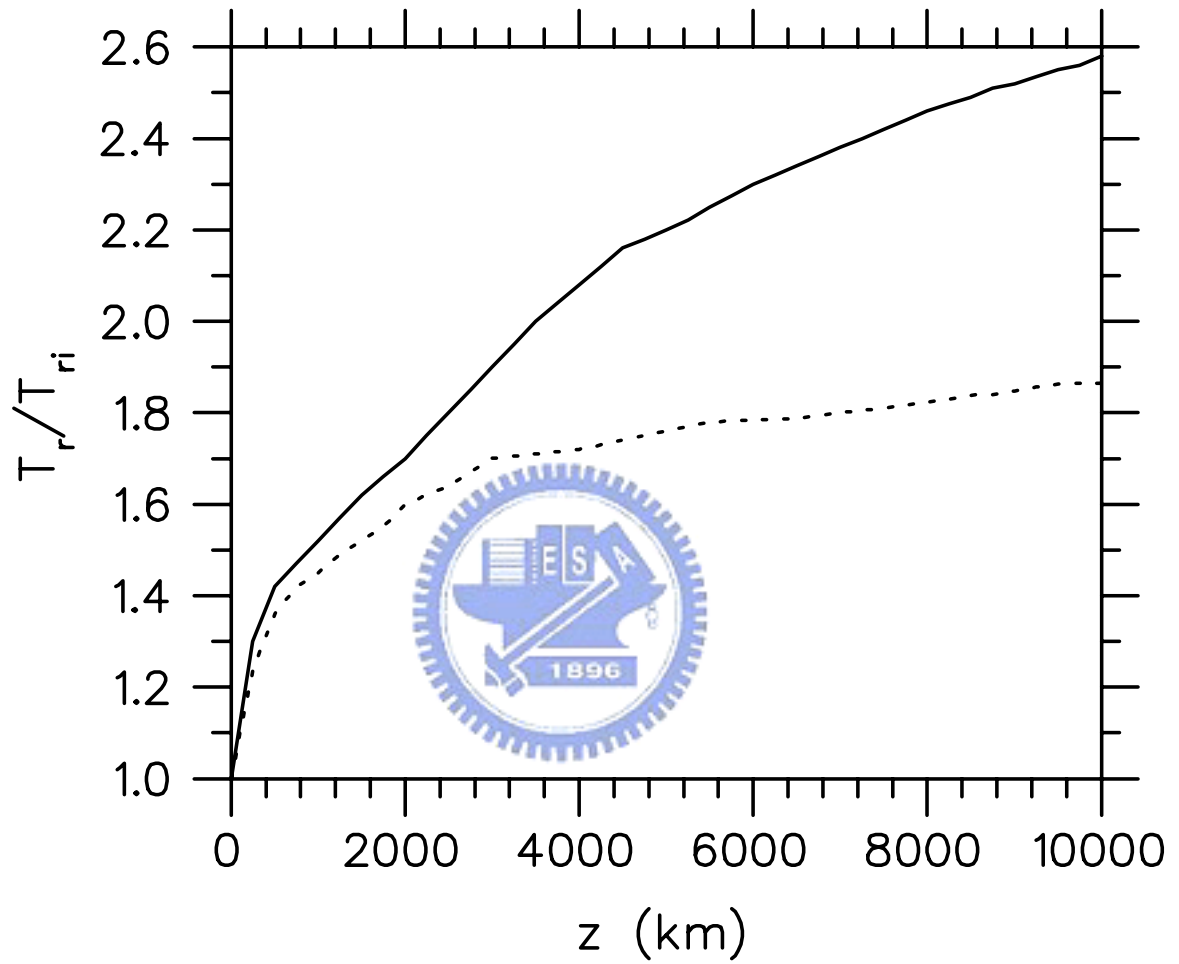


Figure 3.2 (b)

Figure 3.2

(a) The average integrated soliton energy  $\bar{E}_1$ ; (b) the standard deviation of integrated energies  $\delta E_1$ ,  $\delta E'_1$  and  $\delta E_0$ .



**Figure 3.3**

Average rms pulsewidth  $T_r$  normalized by initial value  $T_{ri}$  along the fiber for the case of 10-ps soliton. The cases with and without amplifier noise are shown by solid and dash lines, respectively.

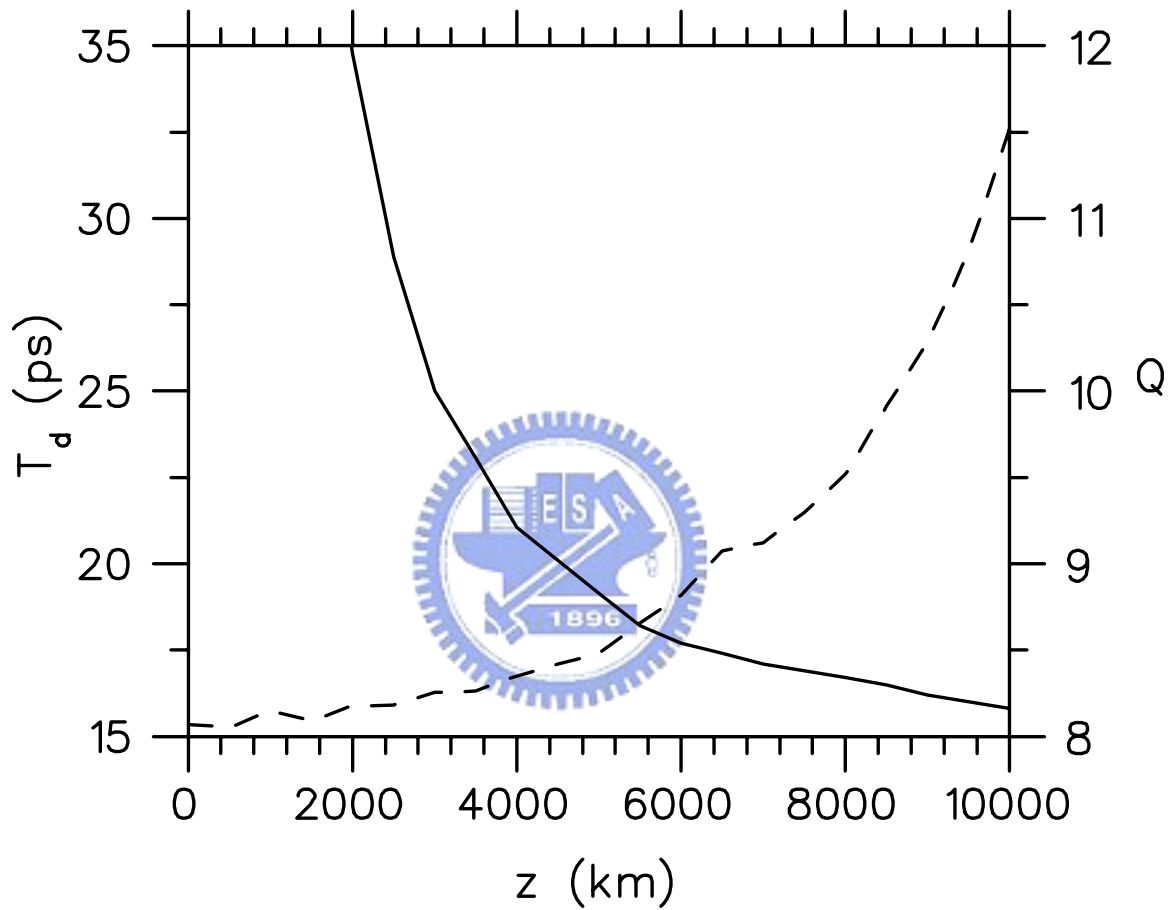


**Figure 3.4**

Optimal detection window  $T_d$  and the corresponding Q factor for different transmission distances for the case of 10-ps soliton.

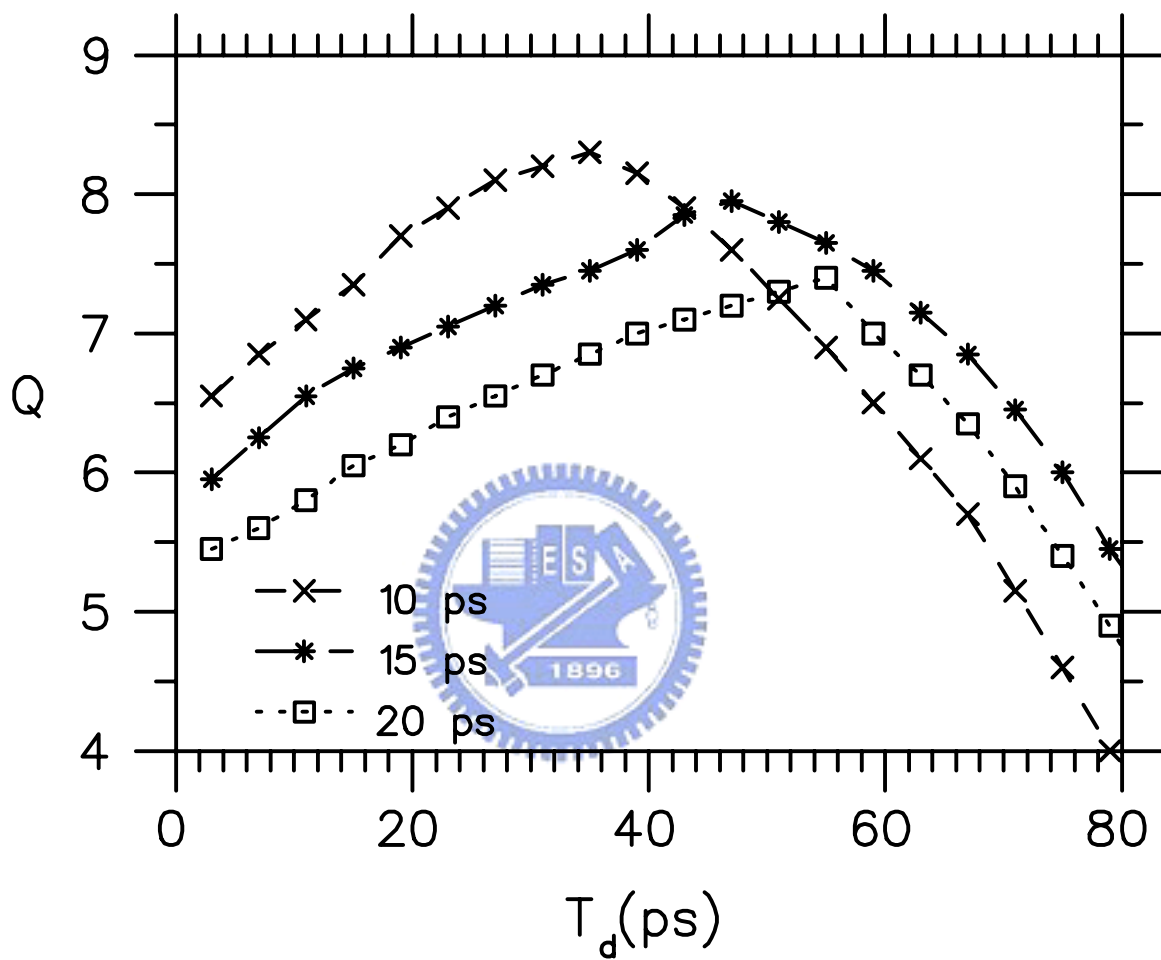


**Figure 3.5**

Q factor versus detection window  $T_d$  for 10-Gbit/s bit rate and 10,000-km transmission distance. The cases of the soliton pulsewidth  $T_s=10$  ps, 15 ps, and 20 ps are shown.

## Chapter 4

# A Stabilization Method for Dispersion-Managed Soliton

Dispersion-managed (DM) soliton transmission systems are interested in recent years [31], [38]. Soliton power can be tailored by arranging dispersion map [37]. Gordon-Haus timing jitter [8] can be nearly eliminated in DM soliton systems. On the other hand, there are drawbacks for DM soliton systems. DM soliton is stable in lossless fiber links. With fiber loss and optical amplifiers for compensating fiber loss, there is dispersive wave generated when DM soliton breathes. There is dispersive wave generated from the resonant sidebands that is due to positive and negative dispersion links. When significant dispersive waves are generated, the pulse shape of DM soliton is degraded and signal to noise ratio is also decreased. Furthermore, the intrachannel interactions between neighboring pulses are enhanced. Third-order fiber dispersion also can enhance the generation of dispersive waves. Secondly, performance of DM soliton system is sensitive to the parameters such as enhanced power, dispersion strength, dispersion map, and amplifier spacing. In lossless case, the methods for designing the system parameters are proposed [39], [40]. But the DM solitons designed with these methods become unstable when there are fiber losses and optical amplifiers.

In this chapter, we propose a method to design the system parameters so that

the stability of DM soliton is improved in the lossy fiber with optical amplifiers. In DM soliton systems, the dispersive wave, timing jitter, and power variation or amplitude jitter degrade system Q value. On the other point of view, this is because Gaussian ansatz assumption is not an exact solution of periodic DM soliton. We consider the case with periodic amplification for compensating fiber loss and the period of dispersion map coinciding the amplification period. The proposed method is the use of proper enhancement power factor and in-line filter bandwidth for every period so that the Gaussian input pulse can slowly evolve into a periodic DM soliton with minimal radiated dispersive waves. Numerical results show that the stability of the DM soliton and the system Q value can be significantly improved.

#### 4.1 Pulse stability control by in-line filter and excess gain

The modified nonlinear Schroedinger equation that describes the soliton propagation in a fiber is described in Eq. 2.1 This equation can be numerically solved with split-step Fourier method as described in Chapter 1. Here we take the carrier wavelength  $\lambda = 1.55 \mu\text{m}$ , the third-order fiber dispersion  $\beta_3 = 0.08 \text{ ps}^3/\text{km}$ , the nonlinearity  $\gamma = 2.4 \text{ W}^{-1}\text{m}^{-1}$ , and the fiber loss  $\alpha = 0.2 \text{ dB/km}$ . 20-Gb/s soliton system is considered, in which soliton pulsewidth (FWHM)  $T_s = 10 \text{ ps}$ . The spontaneous emission factor  $n_{\text{sp}}$  of an an optical amplifier is assumed to be 1.2. The dispersion map is shown in Figure 4.1, in which

$$\langle \beta_2 \rangle = \frac{\beta_{21}L_1 + \beta_{22}L_2}{L_1 + L_2} \quad (4.1)$$

is the path average dispersion. The amplifier spacing is  $L_a = L_1 + L_2$ . An in-line second-order Butterworth filter(BWF) is inserted after every amplifier to reduce the dispersive wave, the amplified spontaneous emission (ASE) noise of amplifier, and the noise-induced timing jitter.

For the conventional soliton system of long transmission links with uniform fiber dispersion, we can use the in-line filters of the same proper bandwidth to filter amplifier noise. In such a case, usually there is slight filtering loss for soliton spectrum. Excess amplifier gain is required to compensate for the filtering loss. The filtering loss leads to the distortion of soliton spectrum. The large power variation during transmission links also perturbs soliton. Fortunately, the robust nature of soliton can adjust itself so that the soliton still remains stable during long haul transmission.

In DM soliton transmission systems, the resonant sidebands and noise induce dispersive waves. In order to reduce this effect, the use of in-line BWFs is not only to filter amplifier noise but also to eliminate the dispersive wave. Therefore higher excess amplifier gain is required to compensate for the filtering loss. In such a situation, DM soliton is not as robust as conventional soliton and DM soliton is not stable with the in-line filters of the same bandwidth. We find that such a DM soliton can be stabilized by respectively optimizing the in-line filter bandwidth  $B$  and the excess gain  $G_e$  for every amplification period.

## 4.2 Numerical results

Take the dispersion map parameters as an example:  $\langle\beta_2\rangle = -0.1 \text{ ps}^2/\text{km}$ ,  $\beta_{21} = -1.0 \text{ ps}^2/\text{km}$ ,  $\beta_{22} = 0.8 \text{ ps}^2/\text{km}$ ,  $L_1 = L_2$ , and  $L_a=80 \text{ km}$ . Figure 4.2 shows the evolution of soliton energy along the transmission links, where  $E_i$  represents the input initial pulse energy and represents the pulse energy at the output of every amplifier. The integration time of pulse energy is  $2T_s$  centered at pulse's center. Line 0 shows the ideal lossless case without optical amplifier (therefore no amplifier noise) and in-line filters. We can see the evolution is stable. As the period of dispersion map is designed to coincide with amplification stage, the pulse evolution is nearly periodic with the period (80km). Line 0 shows the pulse energy  $E_0$  at the end of every unit cell and the periodic variation within a unit cell is not shown. However a 3,400-km long-distance periodic behavior is observed. Line 1 shows the case with amplifier noise but without filters. The pulse breaks up at about 2,000 km and no longer recovers. Line 2 shows the case with the same filter of bandwidth 150 GHz for every amplifier. Pulse is more stable than the case of Line 1. Line 3 shows the same case as Line 2 except that filter bandwidth is set to a larger value of 200 GHz. One can see the pulse is more stable than Line 2 case. In fact we cannot find a filter bandwidth so that the pulse is stable and shows similar long distance periodic characteristic as the ideal lossless case (Line 0). Line 4 shows the case with optimized filter bandwidth and excess gain respectively for every amplification period. The long-distance periodic like evolution appears. For this case, the pulse is stabilized although is not as good as the lossless case. The following describes the method for optimizing the paired parameters, in-line filter



bandwidth  $B$  and the excess gain  $G_e$ , for every amplification period so that DM soliton is stabilized in the presence of fiber loss and optical amplifiers.

We consider a transmission system in which an optical amplifier and an optical filter are located at the end of a unit cell. For optimizing  $B$  and  $G_e$  for the  $n$ -th amplifier, we define the path average pulsewidth variation within  $(n + 1)$ -th amplification period as

$$\delta^2(B, G_e) = \frac{1}{T_s^2 L_a} \int_{nL_a}^{(n+1)L_a} |T(z, B, G_e) - T(z - L_a, B, G_e)|^2 dz, \quad (4.2)$$

where  $T(z, B, G_e)$  is the pulsewidth (FWHM) at a distance of  $z$  with the parameter  $B$  and  $G_e$ . The parameters  $B$  and  $G_e$  are optimized so that is minimized. The evolutions of pulsewidth (FWHM) are shown in Figure 4.3 for the parameters given in Figure 4.2. Line 0 shows the ideal lossless case without amplifier noise and in-line filters. The stable pulsewidth evolution is shown. However, pulse is deteriorated when fiber loss and amplifiers are considered. Line 1 shows such a case without filter. One can see that the pulsewidth dramatically increases with distance mainly because the noisy background significantly results in random phase modulation to the pulse through Kerr effect. With the same filter bandwidth and excess gain for every amplification period, Line 2 and Line 3 also show dramatic increase of pulsewidth with distance, in which the filter bandwidths are 10 times and 15 times the pulse's spectral width, respectively. Although the filter can eliminate dispersive wave, the pulses loose too much energy and become unstable. For both cases, after about 6,500 km, the pulses break up and no longer recover. With the optimized filter bandwidth and excess gain for each amplification period, Line 4 shows the pulse is stable and its evolution is close to the ideal lossless case.

For this optimized case, Figure 4.4 shows the minimum path averaging pulsewidth variation  $\delta$ , the filter bandwidth  $B$  (normalized to 150 GHz), and the excess gain relating parameter  $G_e$ , along the transmission links. In the figure, at 10,000 km,  $B=192$  GHz,  $G_e=1.145$ , and the corresponding  $\delta = 0.28$ . One can see that the values of the three parameters sharply increase at about 7,200 km. After 10,000 km,  $B$  and  $G_e$  reach steady values. Figure 4.5 compares the pulse shapes of the ideal lossless case and the optimized case at 10,000 km, in which the input Gaussian pulse is also shown for comparison. However, from Figure 4.3, one can see that in fact pulsewidth increases in the long run for all the cases shown in this figure. It is noticed, even for the ideal lossless case, the DM soliton also slightly disperses at 10,000 km.

Although the above example shows this method is able to stabilize DM soliton, the stabilization is not guaranteed for any dispersion map. Figure 4.6 shows the Q value of the system optimized with the above method for several dispersion maps. The Q value is evaluated at 10,000 km. All the cases remain the same. That is the amplifier spacing is 80 km. The corresponding dispersion values  $\beta_{21}$  and  $\beta_{22}$  can be easily calculated from the average dispersion and map strength  $S$  as shown in Table 4.1, where

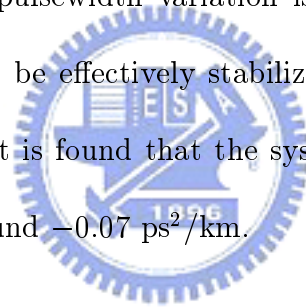
$$S = |\beta_{21}L_1 - \beta_{22}L_2|/T_s^2. \quad (4.3)$$

One can see that Q value is maximal for the average dispersion around  $-0.07$  ps<sup>2</sup>/km and smaller map strength is better for the cases shown in Figure 4.6. If  $\langle\beta_2\rangle$  is too small, DM soliton power is low and signal to noise ratio is poor. If  $\langle\beta_2\rangle$  is too high, DM soliton power is high but more unstable that is due to short local

soliton length. For this case, our method is not able to stabilize DM solitons. The DM soliton is stable with weak map strength, absolute value  $\beta_{21}$  and  $\beta_{22}$  decrease with map strength. Therefore the Q-value in Figure 4.6 increase with weaker map strength.

### 4.3 Summary

In summary, the method to stabilize DM soliton in the presence of fiber loss and optical amplifiers (therefore there is amplifier noise) is presented. We optimize in-line filter bandwidth and the relating excess gain for every amplification period so that the path average pulsewidth variation is minimized. Numerical results show that DM soliton can be effectively stabilized with proper dispersion map. For the considered cases, it is found that the system Q-value is maximized with the average dispersion around  $-0.07 \text{ ps}^2/\text{km}$ .



$S = 0.36$	$\langle \beta_2 \rangle$	$\beta_{21}$	$\beta_{22}$
	-0.02	-0.47	0.43
	-0.04	-0.49	0.41
	-0.06	-0.51	0.39
	-0.08	-0.53	0.37
	-0.10	-0.55	0.35
$S = 0.72$			
	-0.02	-0.92	0.88
	-0.04	-0.94	0.86
	-0.06	-0.96	0.84
	-0.08	-0.98	0.82
	-0.10	-1.0	0.8
$S = 1.52$			
	-0.02	-1.92	1.88
	-0.04	-1.94	1.86
	-0.06	-1.96	1.84
	-0.08	-1.98	1.82
	-0.10	-2.0	1.8
$S = 2.32$			
	-0.02	-2.92	2.88
	-0.04	-2.94	2.86
	-0.06	-2.96	2.84
	-0.08	-2.98	2.82
	-0.10	-3.00	2.80

**Table 4.1**

The dispersion map strength correspondent to different  $\beta_{11}$  and  $\beta_{22}$ ,  $\langle \beta_2 \rangle = -0.1 \text{ ps}^2/\text{km}$ ,  $L_1 = L_2 = 40 \text{ km}$ .

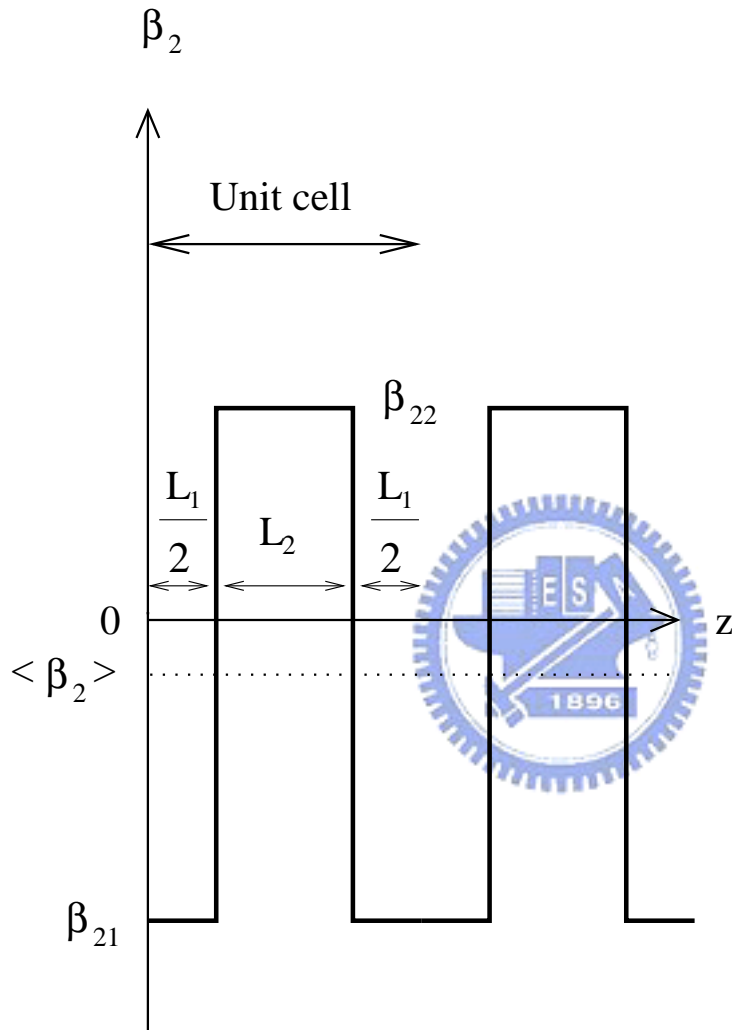


**Figure 4.1**

Dispersion map.  $\langle \beta_2 \rangle$  is the path average dispersion.  $L_1$  and  $L_2$  are the fiber length correspond to the dispersion  $\beta_{21}$  and  $\beta_{22}$ , respectively. The amplifier spacing is  $L_a = L_1 + L_2$ .

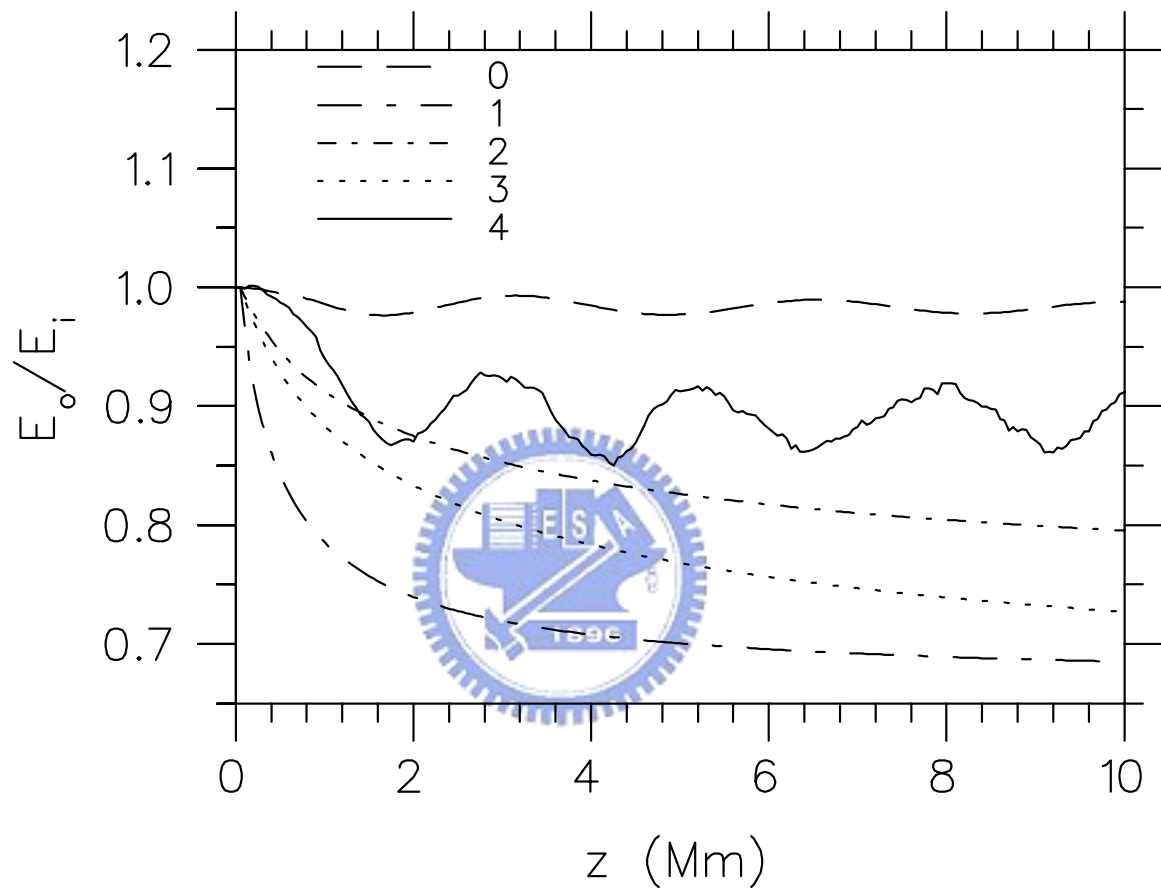


**Figure 4.2**

The evolution of soliton energy along the transmission links, where  $E_i$  represents the input initial pulse energy and represents the pulse energy at the output of every amplifier.

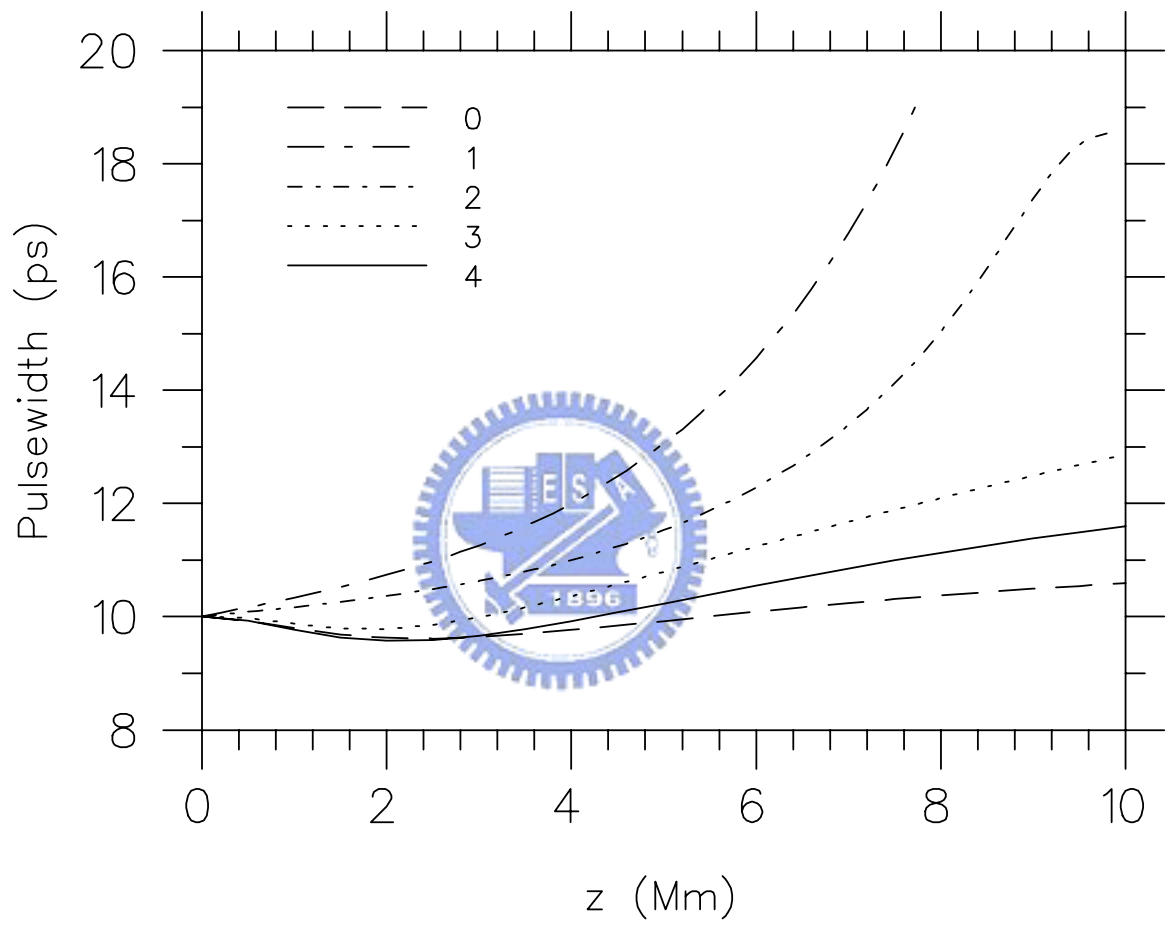


**Figure 4.3**

The evolutions of pulsewidth (FWHM) for the parameters in Figure 4.2.

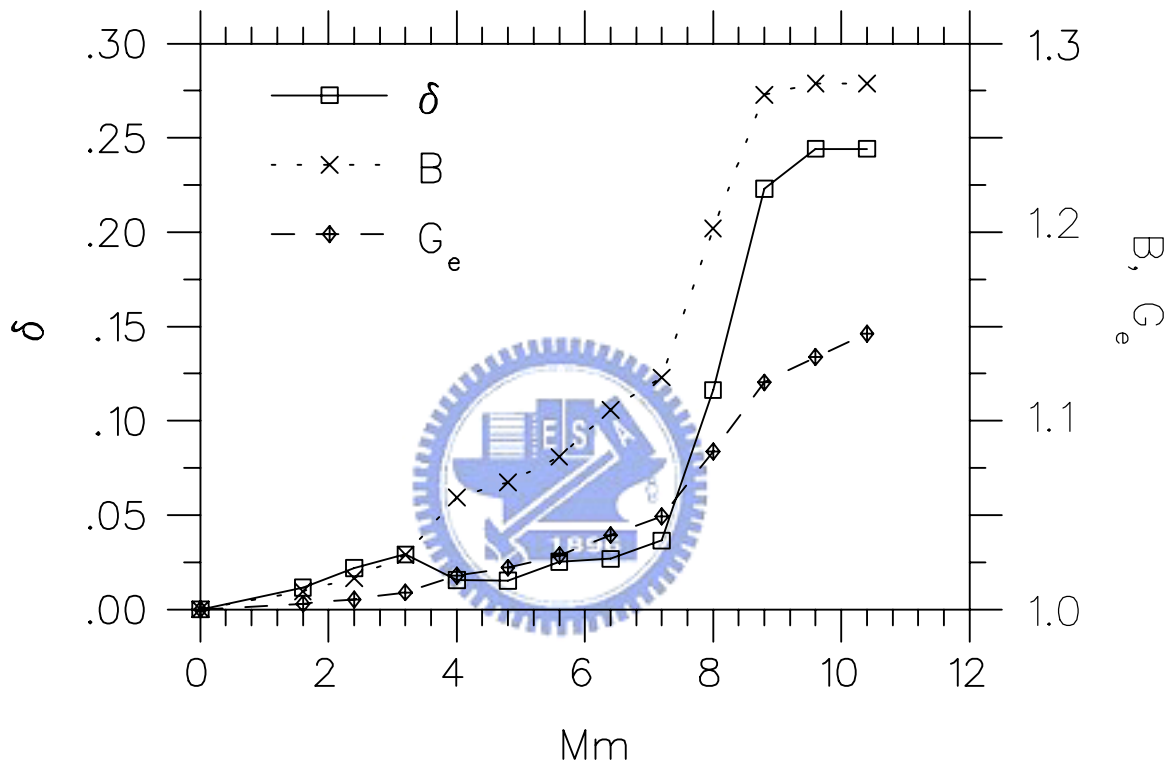


**Figure 4.4**

The minimum path averaging pulsewidth variation  $\delta$ , the filter bandwidth  $B$  (normalized to 150 GHz), and the excess gain  $G_e$ , along the transmission links.



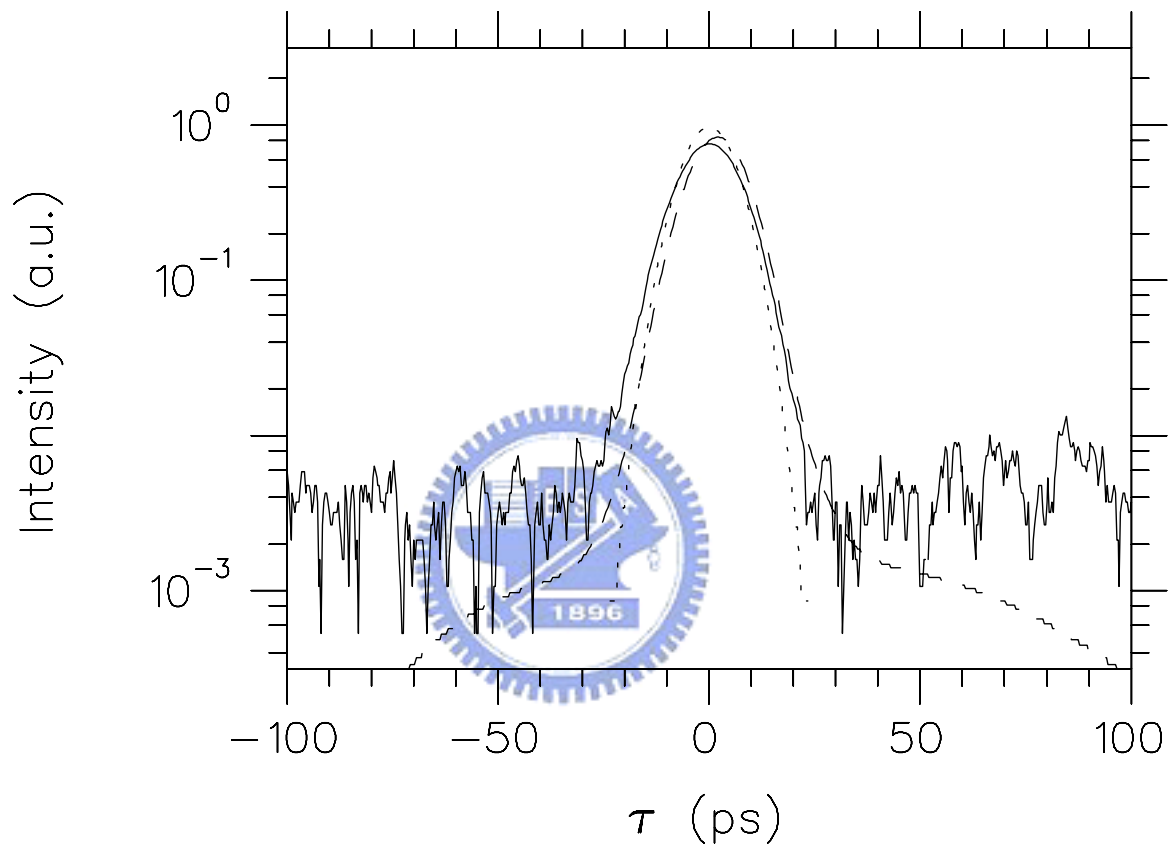


**Figure 4.5**

The pulse shapes of the ideal lossless case (dashed line) and the optimized case (solid line) at 10,000km, in which the input Gaussian pulse (dotted line) is also shown for comparison.

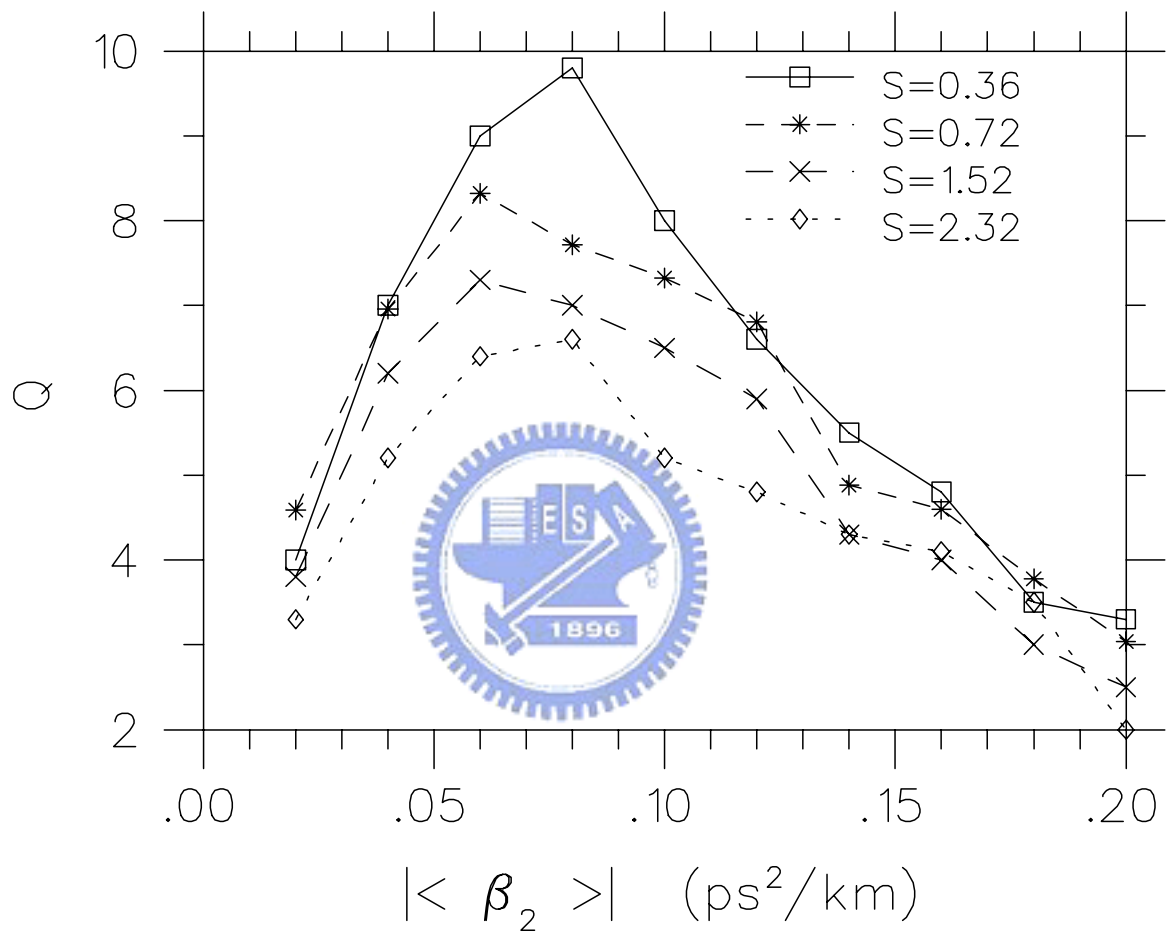


**Figure 4.6**

The Q value of the system optimized with the above method for several dispersion maps.

## Chapter 5

# Post Pulse Compression for Improving Dispersion-Managed Soliton Systems

It is well known that the Gordon-Haus timing jitter [8] can be nearly eliminated in dispersion-managed long-haul soliton transmission systems [29]. The interplay of the breathing nature of DM solitons, large perturbation of system loss in large amplifier spacing, third-order dispersion, and system noise result in dispersive waves in pulse background. If significant dispersive wave is generated, signal to noise ratio is low and DM solitons pulse shape will be degraded seriously. The background noise leads to intrachannel interaction between neighboring pulses. Suitable deployment of filter or sliding filter can efficiently reduce the dispersive wave [34]-[36]. The system performance is also sensitive to the parameters such as enhanced power, dispersion strength, dispersion map, and amplifier spacing [37],[45]. These system performance can be optimized by in-line parameter optimization processes.

In addition to the above in-line improvement methods for DM soliton systems, the systems can also be improved at the receiver. Reference [?] shows that noisy wave can be optically filtered in time domain with the use of optimal width of detection window, which is usually implemented with an optical gate, at receiver. This method is called time domain gating (TDG) method, which is describe in chapter 3. In this chapter, the other method to improve system performance at

receiver is studied. We consider the well-known nature of the frequency chirping of DM solitons and use a dispersive element at receiver to compress DM solitons. A dispersion compensation fiber (DCF) as the dispersive element is used in this chapter. The use of DCF at receiver to compensate for the residual fiber dispersion of transmission system has been widely used in either NRZ or RZ systems and is called post-dispersion compensation (PDC) [46]-[48]. For the DM soliton system, it is more proper to call the use of DCF at receiver as post pulse compression (PPC). We also study the performance improvement of DM soliton systems with PPC and TDG methods at receiver, in which PPC is applied before TDG.

Before applying PPC and TDG methods at receiver, the evolution of DM solitons along the transmission system is designed with a in-line parameter optimization processes. In DM soliton systems, dispersive wave, timing jitter, and power variation or amplitude jitter degrade system Q value. On the other point of view, this is because Gaussian ansatz assumption is not an exact solution of periodic DM soliton with system loss and noise. We carefully choose the enhancement power factor and filter bandwidth so that the Gaussian pulse could slowly evolve into a periodic DM soliton with minimal radiated dispersive wave. The use of PPC is to further reshape the DM soliton's pulse shape but at the cost of more radiated dispersive wave. The dispersive wave can be effectively filtered with TDG. Numerical results show there is significant improvement with PPC. Further improvement can be achieved with TDG.

## 5.1 Theoretical model of post pulse compression

Split-step Fourier method, described in Chapter 1, is used to numerically solve the modified nonlinear Schroedinger equation that describes the soliton propagation in a fiber, as shown in Eq. 2.1. Here we take the carrier wavelength  $\lambda = 1.55 \mu\text{m}$ , the third-order fiber dispersion  $\beta_3 = 0.08 \text{ ps}^3/\text{km}$ , the nonlinearity  $\gamma = 2.4 \text{ W}^{-1}\text{m}^{-1}$ , and the fiber loss  $\alpha = 0.2 \text{ dB/km}$ . The soliton system of 20-Gb/s bit rate is considered, in which soliton pulsewidth full width at half maximum (FWHM)  $T_s = 10 \text{ ps}$ . The spontaneous emission factor of an optical amplifier is assumed to be 1.2. The dispersion map is shown in Fig. 4.1, where  $\langle \beta_2 \rangle$  is the path average dispersion, described in Eq 4.1. The amplifier spacing is  $L_a = L_1 + L_2$ , where  $L_1$  and  $L_2$  are the fiber length correspond to the dispersion  $\beta_{21}$  and  $\beta_{22}$ , respectively. An in-line second-order Butterworth filter (BWF) is inserted after every amplifier to reduce dispersive waves, amplified spontaneous emission (ASE) noise, and noise-induced timing jitter. The filter bandwidth and enhanced power factor are paired parameters. These paired parameters are adjusted or optimized at every amplifier stage [49]. The average dispersion  $\langle \beta_2 \rangle = -0.1 \text{ ps}^2/\text{km}$ ,  $\beta_{21} = -1.0 \text{ ps}^2/\text{km}$ ,  $\beta_{22} = 0.8 \text{ ps}^2/\text{km}$ ,  $L_1 = L_2 = 40 \text{ km}$ , and  $L_a = 80 \text{ km}$ . A 512-bit sequence of psuedo-random Gaussian pulses are input in the DM soliton system. For PPC, a DCF with  $\beta_2 = 80 \text{ ps}^2/\text{km}$ ,  $\beta_3 = 0.1 \text{ ps}^3/\text{km}$ ,  $\alpha = 0.6 \text{ dB/km}$  and  $\gamma = 5.6 \text{ W}^{-1}\text{m}^{-1}$  is used. The length of DCF is optimized for the maximum Q value.

For TDG, the gate function of the detection window is modeled by a fifth-order super-Gaussian function, as in Eq. 3.1 where  $T_d$  is the detection window width and

$m = 5$ . The bit energy is obtained by integrating the amplitude of the filtered signal over a bit's time slot in which its centrum coincides the gate centrum. The system performance can be evaluated via

$$Q = \frac{\mu_1 - \mu_0}{\sigma_1 + \sigma_0}, \quad (5.1)$$

where  $\mu_1$  and  $\mu_0$  are the mean energies of bit ONE and ZERO, and  $\sigma_1$  and  $\sigma_0$  are the standard variations of the energies of bit ONE and ZERO, respectively.

## 5.2 Numerical results

The pulse shape and frequency chirping of a DM soliton after propagating 8,000 km in the system described in the last section are shown in Figure 5.3. One can see that there is nearly anti-symmetric frequency chirping. The maximum positive and negative frequency chirpings are 20 GHz and -30 GHz respectively. A pulse with such frequency chirping can be compressed with the DCF of negative dispersion ( $\beta_2 > 0$ ) at carrier wavelength. System performance can be improved with pulse compression owing to the increase of mean bit energy and the decrease of the standard deviation of bit energy. However, the radiated wave resulting from pulse compression that must be taken case. For the case shown in Figure 5.3, Figure 5.1 shows the pulse shapes for the pulse before applying PPC and after applying PPC. One can see that, as the pulse is compressed with a 0.4 km DCF, there is wave radiated from the pulse. The radiated wave increases with the length of DCF or the ratio of pulse compression. The radiated wave that is due to pulse compression can be effectively filtered with TDG. However, serious radiated wave resulting from

too much pulse compression degrades system performance. Therefore there exists an optimal DCF length or compression ratio.

Figure 5.2 shows the Q value and full width at half maximum (FWHM) pulsewidth with respect to DCF length for 8,000 km transmission distance. For the cases shown in Figure 5.2,  $T_d$  is optimized. One can see that, for the maximum Q value, the FWHM pulsewidth is 12.5 ps and DCF length is 0.4 km. As the FWHM pulsewidth before PPC is 14.5 ps, the optimal compression ratio is 1.16 for this case. Figure 5.4 shows FWHM pulsewidth before applying PPC, and FWHM pulsewidth after applying PPC, and DCF length, as a function of transmission distance for the maximum Q value with optimized  $T_d$ . In the figure shown, for the transmission distance shorter than about 6,000 km, pulsewidth slightly broadens and the optimal pulse compression ration with PPC is small. For the transmission distance longer than about 8,000 km, pulse becomes unstable and there is significant pulse broadening. For such a case, the optimal pulse compression ratio becomes apparent.

Figure 5.5 shows the maximum Q-value with respect to transmission distance for different schemes. Dotted line represents the DM soliton system without any optimization, in which the detection window is the conventional value of one third of a time slot ( $T_d= 16.67$  ps). Dashed line represents the case with optimal PPC and also with  $T_d= 16.67$  ps. Solid line represents the case with both optimal PPC and TDG, in which the value of  $T_d$  is respectively optimized for each transmission. We can see that the improvement of the Q-value with PPC is significant even when the optimal TDG is not applied. For the case without optimal TDG, the

detection window of one third of a time slot is also able to effectively filter the radiation resulting from pulse compression. With the optimal TDG, there is a further improvement.

### 5.3 Summary

The pulse compression with DCF at receiver for improving the Q-value of a DM soliton system is numerically studied. The compression utilizes the nature of frequency chirping of a DM soliton. There is radiated wave resulting from the pulse compression that can be effectively filtered with time domain gating. The results show significant improvement can be achieved with the pulse compression and proper time domain gating. As this technique is simple and is applied at receiver, one can expect that it is promising for upgrade DM soliton system. The overall performance of a wavelength-division-multiplexing (WDM) DM soliton systems also can be expected significantly improved with this technique and is required to be further studied.



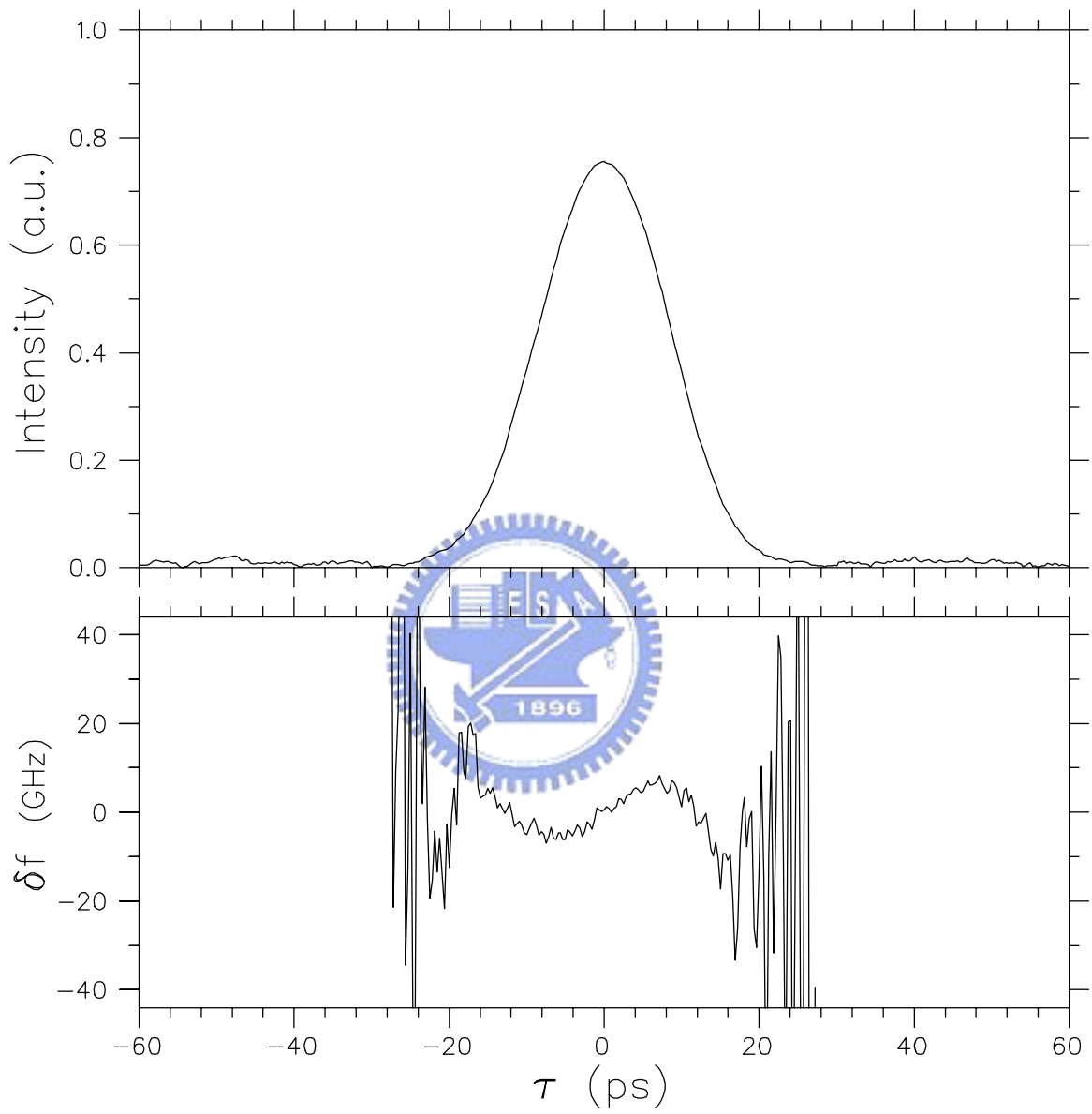


**Figure 5.1**

The pulse shape and frequency chirping of a DM soliton after propagating 8,000 km

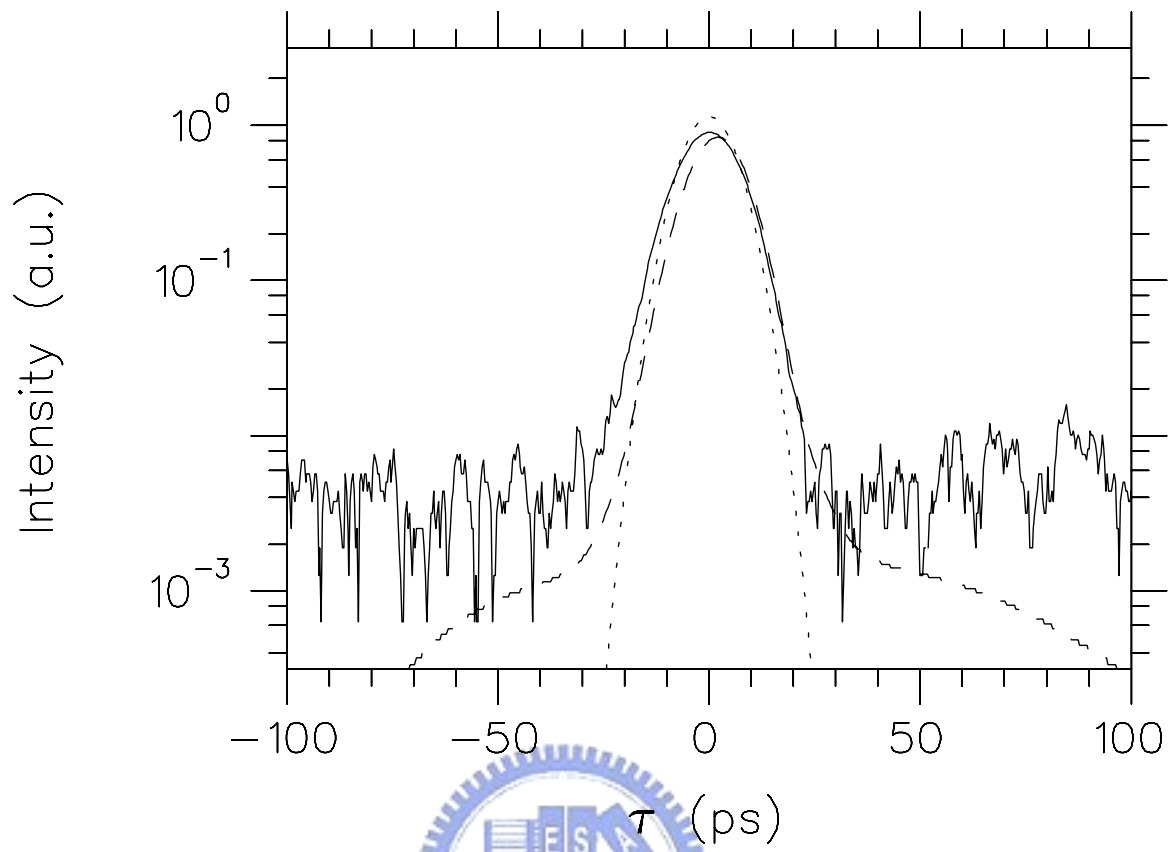


**Figure 5.2**

The pulse shapes for the pulse before (dotted line) applying PPC and after (solid line) applying PPC.

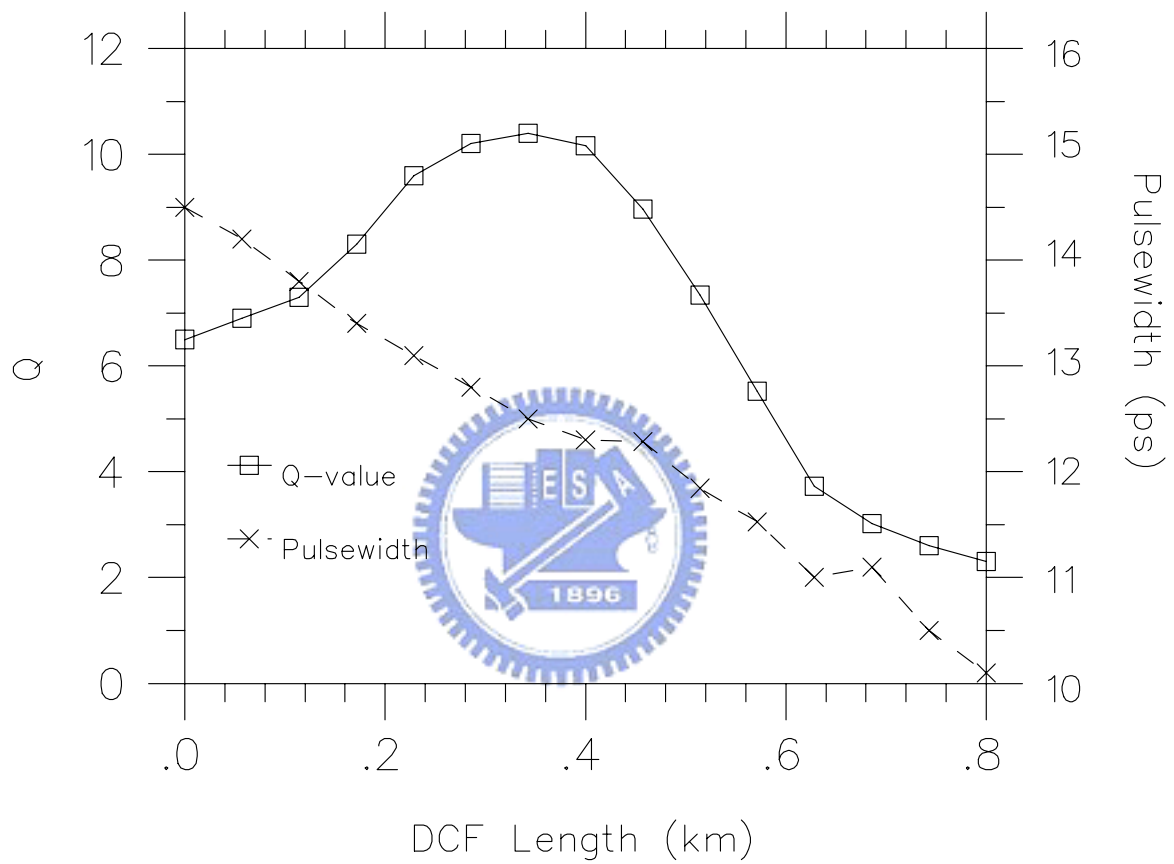


**Figure 5.3**

The Q value and full width at half maximum (FWHM) pulsewidth versus DCF length for 8,000 km transmission distance.

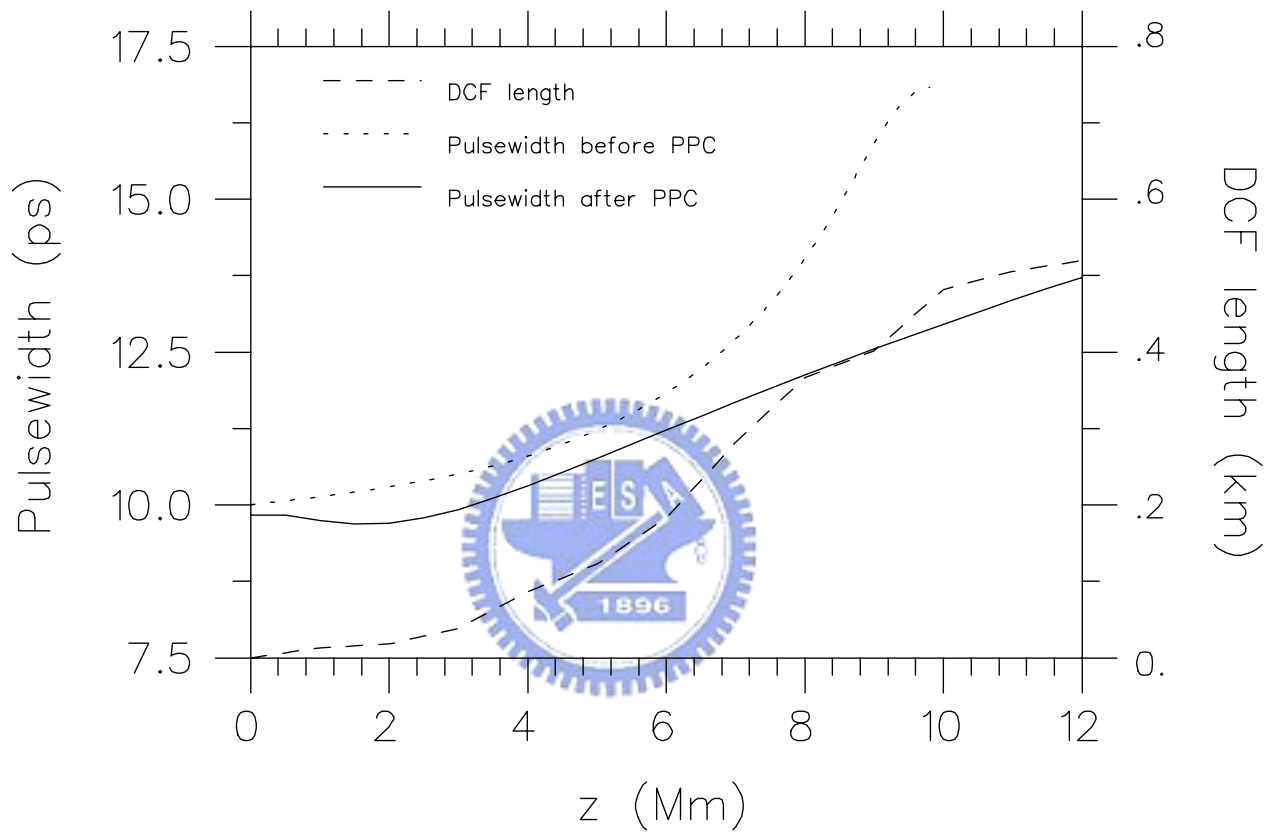


**Figure 5.4**

The FWHM pulsewidth before applying PPC, and FWHM pulsewidth after applying PPC, and DCF length, as a function of transmission distance for the maximum Q value.

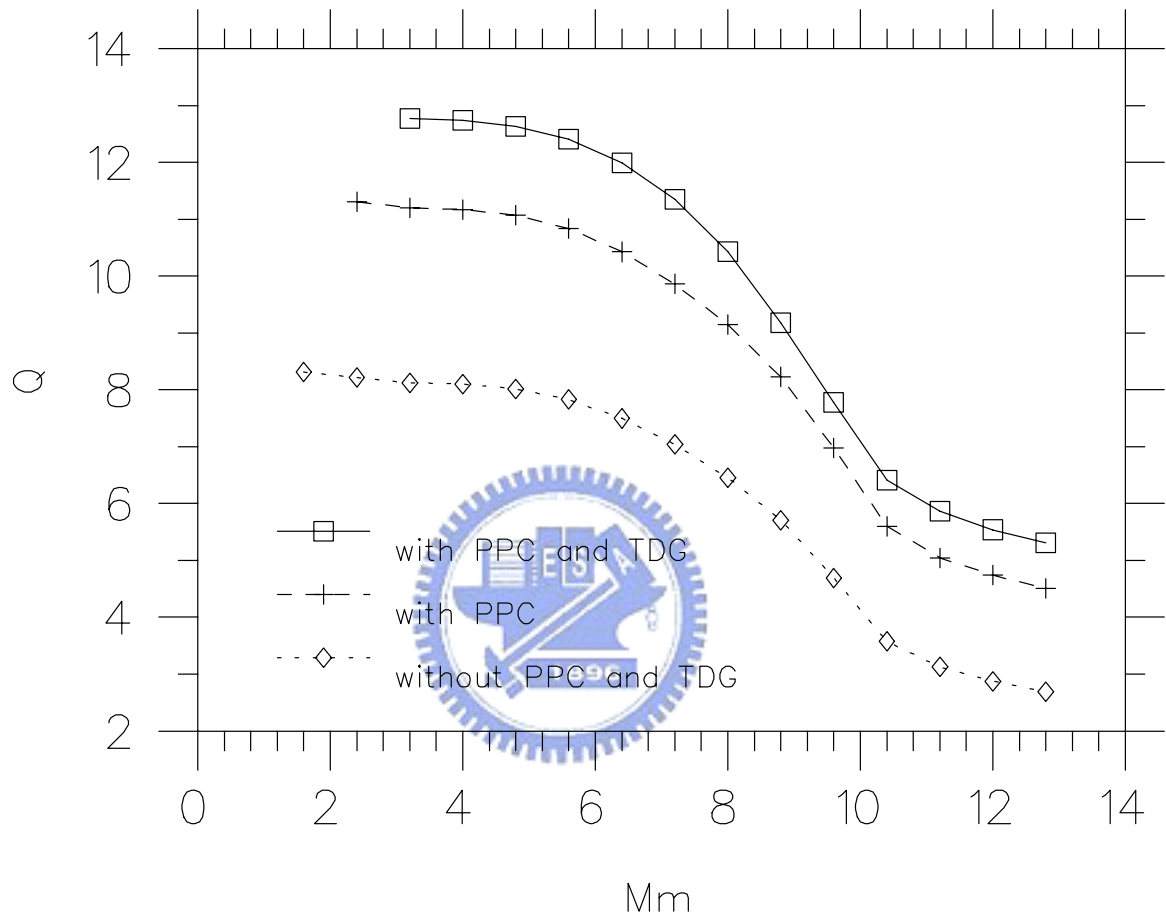


**Figure 5.5**

The maximum  $Q$ -value with respect to transmission distance for different schemes. Dotted line represents the DM soliton system without any optimization. Dashed line represents the case with optimal PPC. Solid line represents the case with both optimal PPC and TDG.

## Chapter 6

### Conclusion

This dissertation deals with the methods for improving the system performance. First we studied the FWM between soliton and amplifier noise in the system with large amplifier spacing, where the DEDF is used as transmission fiber. If fiber dispersion of DEDF is decreased to a small value, the depletion of soliton energy due to the soliton-noise FWM is significant because of the phase matching. On the other hand, if the minimum dispersion of DEDF is large enough, the FWM is reduced but noise-induced timing jitter and soliton-soliton interaction increase. Therefore, there exists the optimum fiber dispersion for the maximum transmission distance. The improvement of the soliton system by using SFF and by compensation of depleted soliton energy is also shown for such a system.

For the soliton detection issue, we found the optimal detection window of a soliton system, which depends on the noise power, noise-induced timing jitter, noise-induced soliton energy fluctuation, dispersive wave, and soliton pulsewidth. The contribution of BER from ONE bits are slightly larger than ZERO bits with the optimal detection window. It is found that the optimal detection window is about three times of the initial soliton pulsewidth for the considered cases.

We proposed a method to design the system parameters so that the stability of DM soliton is improved in the lossy fiber and with optical amplifiers. In DM

soliton systems, dispersive wave, timing jitter, and power variation or amplitude jitter degrade system Q value. On the other point of view, this is because Gaussian ansatz assumption is not an exact solution of periodic DM soliton. We consider the case with periodic amplification for compensating fiber loss and the period of dispersion map coinciding the amplification period. The proposed method is the use of proper enhancement power factor and in-line filter bandwidth for every period so that the Gaussian pulse could slowly evolve into a periodic DM soliton with minimal radiated dispersive waves. Numerical results show that the stability of DM soliton and the system Q value can be significantly improved. It is shown the DM soliton maintains its shape after long transmission with this method. Therefore, the Q-value of the DM soliton system can be significantly improved.

System performance can also be improved with post pulse compression at receiver. DM soliton can be compressed with DCF as a dispersive element owing to its nature of frequency chirping. There is radiated dispersive wave that is due to the compression. The dispersive wave can be effectively filtered with the optical gating in time domain. With proper pulse compression, system Q factor can be significantly improved. This improvement method is simple and it is expected to be implemented in further soliton systems.

In the future, the application of these optimization schemes to the WDM DM soliton system will be investigated, which includes the fine-tuning of system parameters such as in-line filter bandwidth, optical amplifier excess gain, post pulse compression ratio, and detection window width. We will also apply our optimization schemes to the WDM soliton systems pumped by Raman amplifiers [50]-[52].

The Raman gain slope is expected to be a key factor in fine-tuning the system parameters.





## References

- [1] G. P. Agrawal, *Nonlinear Fiber Optics*. London: Academic Press, 2nd ed., 1995.
- [2] L. F. Mollenauer, R. H. Stolen, and J. P. Gordon, "Experimental observation of picosecond pulses narrowing and solitons in optical fibers", *Phys. Rev. Lett.*, vol. 45, pp. 1095-1098, 1980.
- [3] E. Desurvire, *Erbium-Doped Fiber Amplifiers: Principles and Applications*. New York, NY: Wiley, 1994.
- [4] A. Hasegawa, "Amplification and reshaping of optical soliton in glass fiber-IV", *Opt. Lett.* vol. 8, pp 650-652, 1983.
- [5] T. Otani, M. Hayashi, M. Daikoku, K. Ogaki, Y. Nagao, K. Nishijima, M. Suzuki, M., "Field trial of 63 channels 40 Gbit/s dispersion-managed soliton WDM signal transmission over 320 km NZ-DSFs ", *J. Lightwave Technol.* , vol. 22, pp. 208-214, 2004.
- [6] Leclerc, O., Lavigne, B., Balmeffre, E., Brindel, P., Pierre, L., Rouvillain, D., Seguneau, F., "Optical regeneration at 40 Gb/s and beyond", *J. Lightwave Technol.* , vol. 21, pp. 2779-2790, 2003.
- [7] A. Hasegawa, "Numerical study of optical soliton transmission amplified periodically by the stimulated Raman process", *Appl. Opt.* vol. 23, pp 3302-3309, 1984.
- [8] J. P. Gordon and H. A. Haus, "Random walk of coherently amplified solitons in optical fiber transmission", *Opt. Lett.* , vol. 11, pp. 665-667, 1986.
- [9] L. F. Mollenauer, J. P. Gordon and M. N. Islam, "Soliton propagation in long fibers with periodically compensated loss ", *IEEE J. Quantum Electron.*, vol. 22, pp. 157-162, 1986.

- [10] A. Hasegawa, Y. Kodama, “Guiding-center soliton” *Phys. Rev. Lett.*, vol. 66, pp. 161-164, 1991.
- [11] S. M. J. Kelly, K. Smith, K. J. Blow, N. J. Doran, “Average soliton dynamics of a high-gain erbium fiber laser” *Optics Lett.*, vol. 16 pp. 1337-1339, 1991.
- [12] Jean-Pierre Hamaide, Elisabeth Brun, Olivier Audouin, Bernard Biotteau, “Experimental demonstration of second-order average soliton propagation in an optical fiber over several soliton periods” *Optics Lett.*, vol. 19 pp. 25-27, 1994.
- [13] W. Forysiak, F. M. Knox, N. J. Doran , “Average soliton propagation in periodically amplified systems with stepwise dispersion-profiled fiber” *Optics Lett.*, vol. 19 pp. 174-176, 1994.
- [14] A. Mecozzi, “Long-distance transmission at zero dispersion: Combined effect of the Kerr nonlinearity and the noise of the in-line amplifiers”, *J. Opt. Soc. Am. B*, vol. 11, pp. 462-469, 1994.
- [15] K. Tajima, “Compensation of soliton broadening in nonlinear optical fibers with loss”, *Opt. Lett.*, vol. 12, pp. 54-56, 1987.
- [16] S. Chi, C.-Y. Kao, and S. Wen, “Four-Wave Mixing between a Soliton and Noise in a System with Large Amplifier Spacing”, *Opt. Lett.*, vol. 22, pp. 1636-1638, 1997.
- [17] A. Mecozzi, J. D. “Soliton transmission control”, Moores, H. A. Haus, and Y. Lai. *Opt. Lett.*, vol. 16, pp. 1841-1843, 1991.
- [18] F. Matera, J. Settembre, “Comparison of the performance of optically amplified transmission systems”, *J. Lightwave Technol.*, vol. 14 pp. 1-11, 1996.
- [19] D. S. Govan, W. Forysiak, N. J. Doran, “Long-distance 40-Gbitssoliton transmission over standard fiber by use of dispersionmanagement”, *Opt. Lett.*, vol. 23, pp 1523-1525, 1998.
- [20] L. F. Mollenauer, J. P. Gordon, and S. G. Evangelides, “The sliding-frequency guiding filter: an improved form of soliton jitter control”, *Opt. Lett.*, vol. 17, 1575-1577, 1992.

- [21] N. S. Bergano, F. W. Kerfoot, C. R. Davidson, "Margin measurements in optical amplifier system", *IEEE Photon. Technol. Lett.*, vol. 5, pp. 304-306, 1993.
- [22] R. Holzlohner, V. S. Grigoryan, C. R. Menyuk, and W. L. Kath, "Accurate calculation of eye diagrams and bit error rates in long-haul transmission systems using linearization", *J. Lightwave Technol.*, vol. 20, pp. 389-400, 2002.
- [23] D. Marcuse, "Derivation of analytical expressions for the bit-error probability in lightwave systems with optical amplifiers", *J. Lightwave Technol.*, vol. 8, pp. 1816- 1823, 1990.
- [24] D. Marcuse, "Calculation of bit-error probability for a lightwave system with optical amplifiers and post-detection Gaussian noise", *J. Lightwave Technol.*, vol. 9, pp. 505-513, 1991.
- [25] M. Suzuki, H. Tanaka, N. Edagawa, Y. Matsushima, "New applications of a sinusoidally driven InGaAsP electroabsorption modulator to in-line optical gates with ASE noise reduction effect", *J. Lightwave Technol.*, vol. 10, pp. 1912-1918, 1992.
- [26] M. Suzuki, H. Tanaka, Y. Matsushima, "10 Gbit/s optical demultiplexing and switching by sinusoidally driven InGaAsP electroabsorption modulators", *Electron. Lett.*, vol. 28 pp. 934-935, 1992.
- [27] M. Suzuki, N. Edagawa, I. Morita, S. Yamamoto, S. Akiba, "Soliton-based return-to-zero transmission over transoceanic distances by periodic dispersion compensation", *J. Opt. Soc. Am. B*, vol. 14, pp. 2953-2959, 1997.
- [28] G. P. Agrawal, *Fiber-Optic Communication Systems*, 2nd ed., New York: John Wiley, 1997, Chapter 4.
- [29] A. Berntson, N. J. Doran, W. Forysiak, J. H. B. Nijhof "Power dependence of dispersion-managed solitons for anomalous, zero, and normalpath-average dispersion", *Opt. Lett.* vol. 23, pp. 900-902, 1998.
- [30] N. J. Smith, N. J. Doran, F. M. Knox, and W. Forysiak, "Energy-scaling characteristics of solitons in strongly dispersion-managed fibers", *Opt. Lett.*, vol. 21, pp. 1981-1983, 1996.

- [31] N. J. Smith, N. J. Doran, W. Forysiak, F. M. Knox, “Soliton transmission using periodic dispersion compensation”, *J. Lightwave Technol.*, vol. 15, pp. 1808-1822, 1998.
- [32] N. J. Smith, N. J. Forysiak, and W. Doran, “Reduced Gordon-Haus jitter due to enhanced power solitons in strongly dispersion managed systems”, *Electron. Lett.*, vol. 32, pp. 2085-2086, 1996.
- [33] Y. Kodama, M. Romagnoli, and S. Wabnitz, “Chirped nonlinear pulse propagation in a dispersion-compensated system”, *Opt. Lett.*, vol. 22, pp. 1689-1691, 1997.
- [34] Matsumoto, M., “Effects of guiding filters on stretched-pulse transmission in dispersion-managed fibres”, *Electron. Lett.*, vol. 33, pp. 1718-1720, 1997.
- [35] Ferreira, M.F.S., Sousa, M.H., “Timing jitter of dispersion-managed solitons controlled by filters: analytical results”, *Electron. Lett.*, vol. 37, pp. 1184-1185, 2001.
- [36] Carter, G.M., Jacob, J.M., “Dynamics of solitons in filtered dispersion-managed systems”, *IEEE Photon. Technol. Lett.*, vol. 10, pp. 546-548, 1998.
- [37] S. K. Turitsyn, M. P. Fedoruk, E. G. Shapiro, V. K. Mezenrsev, E. G. Turitsyna, “Novel approaches to numerical modeling of periodic dispersion-managed fiber communication systems”, *J. Quantum Electron.*, vol. 6, pp. 263-275, 2000.
- [38] N. J. Smith, F. M. Knox, N. J. Doran, K. J. Blow, I. Bennion, “Enhanced power solitons in optical fibres with periodic dispersion management”, *Electron. Lett.*, vol. 32 pp. 54-55, 1996.
- [39] S. K. Turitsyn, M. P. Fedoruk, E. G. Shapiro, “Novel approaches to numerical modeling of periodic dispersion-managed fiber communication systems”, V. K. Mezenrsev, E. G. Turitsyna, *J. Quantum Electron.*, vol. 6, pp. 263-275, 2000.
- [40] J. H. B. Nijhof, W. Forysiak, N. J. Doran, “The averaging method for finding exactly periodic dispersion-managed solitons”, *J. Quantum Electron.*, vol. 6, pp. 330-336, 2000.

- [41] T. Schafer, E. W. Laedke, M. Gunkel, C. Karle, "Optimization of dispersion-managed optical fiber lines", A. Posth, K. H. Spatschek, S. K. Turitsyn, *J. Lightwave Technol.*, vol. 20, pp. 946-952, 2002.
- [42] C. Peucheret, N. Hanik, R. Freund, L. Molle, P. Jeppesen, "Optimization of pre- and post-dispersion compensation schemes for 10-Gbits/s NRZ links using standard and dispersion compensating fibers", *IEEE Photon. Technol. Lett.*, vol. 12, pp. 992-994, 2002.
- [43] S. Chi, C.-Y. Kao, J.-C. Dung, S. Wen, "Adjusting the detection window to improve the soliton communication system", *Optics Comm.*, vol. 186, pp. 99-103, 1997.
- [44] N. J. Smith, F. M. Knox, N. J. Doran, K. J. Blow, I. Bennion, "Enhanced power solitons in optical fibres with periodic dispersion management", *Electron. Lett.*, vol. 32 (1996)54-55.
- [45] A.-D. Capobianco, A. Tonello, S. Wabnitz, O. Leclerc, B. Dany, E. Pincemin, "Stability analysis of dispersion-managed soliton propagation with reamplification, reshaping, and retiming all-optical regeneration", *J. Opt. Soc. Amer. B.*, vol. 19, pp. 1264-1274, 2002.
- [46] T. Schäfer, E. W. Laedke, M. Gunkel, C. Karle, "Optimization of dispersion-managed optical fiber lines", A. Posth, K. H. Spatschek, S. K. Turitsyn, *J. Lightwave Technol.*, vol. 20, pp. 946-952, 2002.
- [47] R. S. Kaler, A. K. Sharma, T. S. Kamal, "Comparison of pre-, post- and symmetrical-dispersion schemes for 10 Gb/s NRZ links using standard and dispersion compensated fiber", *Optics Comm.*, vol. 209, pp. 107-123, 2002.
- [48] C. Peucheret, N. Hanik, R. Freund, L. Molle, P. Jeppesen, "Optimization of pre- and post-dispersion compensation schemes for 10-Gbits/s NRZ links using standard and dispersion compensating fibers", *IEEE Photon. Technol. Lett.*, vol. 12, pp. 992-994, 2000.
- [49] C.-Y. Kao, S. Wen, S. Chi, "A stabilization method for dispersion-managed soliton in the lossy fiber links of periodic amplification", to be submitted to *Optics Comm.*

- [50] R.-M. Mu and C. R. Menyuk, “Symmetric slope compensation in a long-haul WDM system using the CRZ format”, *IEEE Photon. Technol. Lett.*, vol. 13, pp. 797-799, 2001.
- [51] Del Duce, A., Killey, R.I. Bayvel, P., “Comparison of nonlinear pulse interactions in 160-Gb/s quasi-linear and dispersion managed soliton systems”, *J. Lightwave Technol.*, vol. 20, pp. 946-952, 2002.
- [52] Pizzinat, A.; Santagiustina, M.; Schivo, C.; “Impact of hybrid EDFA-distributed Raman amplification on a 4x40-Gb/s WDM optical communication system”, *IEEE Photon. Technol. Lett.*, vol. 15, pp. 341-343, 2003.



## Published Work

1. Sien Chi, Chuan-Yuan Kao, and Senfar Wen,  
“Four-Wave Mixing between a Soliton and Noise in a System with  
Large Amplifier Spacing”,  
*Opt. Lett.*, vol. 22, pp. 1636-1638, 1997.
2. Sien Chi, Chuan-Yuan Kao, Jeng-Cherng Dung, and Senfar Wen,  
“Adjusting the Detection Window to Improve the Soliton Commu-  
nication System”,  
*Opt. Comm.*, vol. 186, pp. 99-133, 2000



# 簡 歷

## (Vita)

姓名：高川原

性別：男

出生年月日：53 年 9 月 7 日

學歷：

1983 – 1987	國立成功大學	物理系	學士
1987 – 1989	國立成功大學	物理系	碩士班
1994 – 2004	國立交通大學	光電所	博士班

經歷：

1991 – 2004	私立中華大學	講師
-------------	--------	----

通訊地址：新竹市 300 東香里六鄰東香 30 號 私立中華大學電機系

E-mail: [kao@chu.edu.tw](mailto:kao@chu.edu.tw)

